Nucleic Acids Research, 2024, **52**, 11785–11805
https://doi.org/10.1093/nar/gkae785
Advance access publication date: 18 September 2024
Genome integrity, repair and replication

Polyubiquitinated PCNA triggers SLX4-mediated break-induced replication in alternative lengthening of telomeres (ALT) cancer cells

Sangin Kim [1,2], Su Hyung Park [1,3], Nalae Kang [1], Jae Sun Ra [1], Kyungjae Myung [1,3,*] and Kyoo-young Lee [1,4,*]

[1]Center for Genomic Integrity, Institute for Basic Science, Ulsan 44919, Korea
[2]Department of Biological Sciences, College of Information-Bio Convergence Engineering, Ulsan National Institute of Science and Technology, Ulsan 44919, Korea
[3]Department of Biomedical Engineering, College of Information-Bio Convergence Engineering, Ulsan National Institute of Science and Technology, Ulsan 44919, Korea
[4]Department of Biochemistry, College of Medicine, Hallym University, Chuncheon 24252, Gangwon-do, Republic of Korea

*To whom correspondence should be addressed. Tel: +82 33 248 2543; Email: kylee@hallym.ac.kr
Correspondence may also be addressed to Kyungjae Myung. Email: kmyung@ibs.re.kr

Abstract

Replication stresses are the major source of break-induced replication (BIR). Here, we show that in alternative lengthening of telomeres (ALT) cells, replication stress-induced polyubiquitinated proliferating cell nuclear antigen (PCNA) (polyUb-PCNA) triggers BIR at telomeres and the common fragile site (CFS). Consistently, depleting RAD18, a PCNA ubiquitinating enzyme, reduces the occurrence of ALT-associated promyelocytic leukemia (PML) bodies (APBs) and mitotic DNA synthesis at telomeres and CFS, both of which are mediated by BIR. In contrast, inhibiting ubiquitin-specific protease 1 (USP1), an Ub-PCNA deubiquitinating enzyme, results in an increase in the above phenotypes in a RAD18- and UBE2N (the PCNA polyubiquitinating enzyme)-dependent manner. Furthermore, deficiency of ATAD5, which facilitates USP1 activity and unloads PCNAs, augments recombination-associated phenotypes. Mechanistically, telomeric polyUb-PCNA accumulates SLX4, a nuclease scaffold, at telomeres through its ubiquitin-binding domain and increases telomere damage. Consistently, APB increase induced by Ub-PCNA depends on SLX4 and structure-specific endonucleases. Taken together, our results identified the polyUb-PCNA-SLX4 axis as a trigger for directing BIR.

Graphical abstract

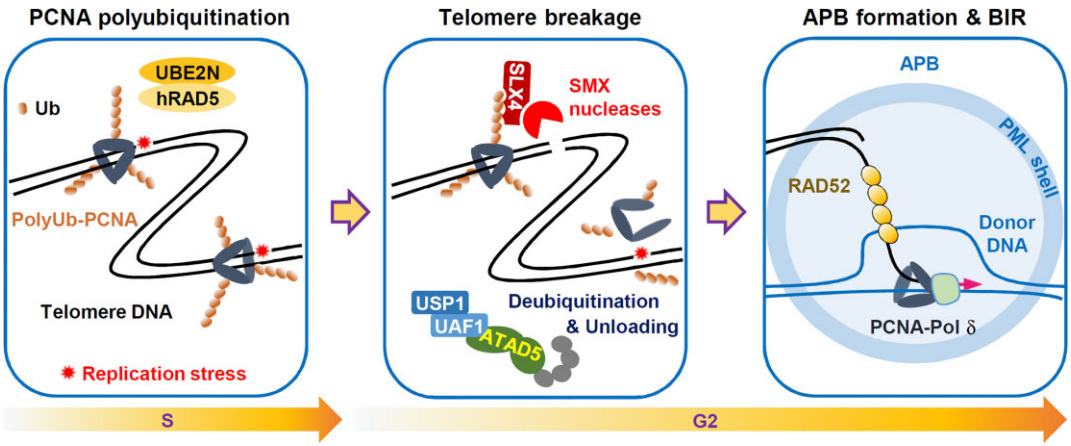

Introduction

Eukaryotic somatic cells undergo telomere shortening during multiple rounds of DNA replication due to loss of telomerase (TEL) activity, which adds the TTAGGG sequence to the end of chromosomes (1,2). The majority of human cancers maintain telomere length by restoring TEL activity (3). Furthermore, 10–15% of human cancers adopt a recombination-dependent alternative lengthening of

Received: September 4, 2023. **Revised:** August 23, 2024. **Editorial Decision:** August 25, 2024. **Accepted:** August 29, 2024

telomeres (ALT) pathway instead of TEL activity (4,5). ALT involves conservative telomeric DNA synthesis via a break-induced replication (BIR) dependent on POLD3 and RAD52 recombinase (6–12). ALT + cancer cells feature ALT-associated promyelocytic leukemia (PML) body (APB), containing telomere clusters and proteins for recombination and DNA synthesis (7–9,13,14).

Replication stress affects difficult-to-replicate regions like common fragile sites (CFSs) or telomeres (15–17). Under mild replication stress, the cells maintain continued DNA replication throughout G2 to resolve replication intermediates (18). However, when cells enter mitosis with incomplete DNA replication under replication stress, RAD52-dependent BIR-like mitotic DNA synthesis (MiDAS) can occur, particularly in CFS (19). Telomeric replication stress leads to telomere clustering and also BIR-like MiDAS at telomeres (8,20).

Telomeric R-loop and G-quadruplex (G4) levels are higher in ALT + cells compared to TEL + cancer cells (21). Despite evidence that telomeric replication stresses trigger ALT activity (21–27), it is unclear how replication stress results in the telomere breakage required to initiate the BIR-associated ALT process.

The eukaryotic sliding clamp proliferating cell nuclear antigen (PCNA), which is loaded on to DNA by the pentameric replication factor C (RFC) complex, is critical for DNA replication and repair (28). It undergoes monoubiquitination at the lysine 164 (K164) residue by the RAD6-RAD18 complex in response to replication stress, recruiting translesion synthesis (TLS) polymerases for error-prone DNA lesion bypass (29). PCNA can also undergo lysine 63 (K63)-linked polyubiquitination by the UBE2N/MMS2 ubiquitin-conjugating dimer and yeast Rad5 ubiquitin ligase homologues, promoting error-free DNA damage tolerance through template switching (29–31).

ATAD5 (human ortholog of yeast Elg1)-RFC-like complex (RLC) unloads PCNA and Ub-PCNA and facilitates PCNA deubiquitination by recruiting the ubiquitin-specific protease 1 (USP1)/USP1-associated factor (UAF1) complex (32–35). ATAD5 is important for faithful DNA replication and repair and for maintaining genomic stability by preventing PCNA/Ub-PCNA accumulation on chromatin (33,35–40). ATAD5 was also reported to be involved in regulating telomere length. Elg1 loss resulted in telomere elongation (41,42), which was rescued by PCNA disassembly-prone mutants or mutation of PCNA K164 to arginine (K164R) (43), suggesting a role for PCNA or Ub-PCNA in promoting telomere elongation.

PCNA ubiquitination is involved in the DNA synthesis step of BIR. The yeast *rad18Δ* mutants or PCNA K164R mutants reduced endonuclease-induced BIR repair (44), suggesting that Ub-PCNA contributes to efficient BIR. In human cells, it was recently reported that RAD18-mediated PCNA ubiquitination and subsequent recruitment of TLS polymerases REV1 and REV3 are required for MiDAS (45). In addition, RAD18-dependent PCNA ubiquitination has been reported to promote resection-dependent template switching during break-induced telomere synthesis (46). However, the role of Ub-PCNA in other steps of BIR, such as break induction and BIR initiation, and the specific involvement of polyUb-PCNA in the BIR-associated ALT process remain unclear. Here, we investigated the effects of modulating ATAD5-USP1 activity specifically in the G2 phase of ALT + cancer cells to determine how Ub-PCNA contributes to the BIR process and BIR-associated ALT phenotypes.

Materials and methods

Cell lines and cell culture

HeLa, HeLa-LT (kindly provided by Dr. Jan Karlseder), GM0637, SK-LU-1, U2OS, U2OS-ATAD5^{AID} (37) and HeLa-ATAD5^{AID} (38) cells were cultured in DMEM (Hyclone) supplemented with 10% fetal bovine serum (Hyclone), 100 U/ml penicillin G (Life Technologies) and 100 mg/ml streptomycin (Life Technologies) in a humidified atmosphere of 5% CO_2 at 37°C. The RAD52-inducible *RAD52*$^{-/-}$ U2OS cells (7) (kindly provided by Dr. Lee Zou) and U2OS-Tet-On-destabilization domain (DD)-estrogen receptor (ER)-mCherry-TRF1-FokI cells (U2OS-mCherry-TRF1-FokI) cells (47) (kindly provided by Dr. Roger A. Greenberg) were cultured in DMEM supplemented with 10% tetracycline-free fetal bovine serum (Takara) and antibiotics. RAD52 protein expression was induced in *RAD52*$^{-/-}$ U2OS cells by treating with 100 ng/ml doxycycline for 48 h. The *ATAD5*$^{-/-}$ U2OS, *ATAD5*$^{-/-}$ SK-LU-1, and *ATAD5*$^{-/-}$ HeLa-LT cell lines were generated using commercial ATAD5 CRISPR/Cas9 knockout plasmids (sc-405654) (Santa Cruz). Briefly, cells were transfected with the CRISPR/Cas9 plasmids, and, after 48 h transfection, GFP-positive cells were sorted using a FACSAria cell sorter (BD biosciences). After 3 weeks, single cell colonies were picked, and complete *ATAD5* knockout was confirmed by immunoblotting. The U2OS cells expressing GFP-tagged full-length SLX4, N-terminal fragment of SLX4 (SLX4^{N}) and SLX4^{N} with a mutation in UBZ4-1, UBZ4-2 or both UBZ4 domains, respectively, were generated using the CSII-CMV-based lentiviral vectors reported in a previous study (48). Briefly, the lentiviral vectors encoding each SLX4 cDNA (kindly provided by Dr. Minoru Takata) were individually co-transfected with two assistant vectors pMD2.G (#12 259, Addgene) and psPAX2 (#12 260, Addgene) into HEK293-FT cells. After 48 h, viral supernatants were collected and clarified by using a 0.2 μm filter. The lentivirus was then infected into U2OS cells with polybrene (sc-134220, Santacruz) followed by selection with 3 μg/ml of blasticidin (R21001, Thermo Fisher) for 5 days. Transfection of plasmid DNA was performed using X-tremeGENE™ HP (Roche) and 20 nM siRNAs were transfected using RNAiMAX (Thermo Fisher). Cells were analyzed 48 h after transfection.

siRNAs

The following synthetic duplex siRNAs were purchased from Bioneer: ATAD5 3′ UTR (5′-GUAUA UUUCU CGAUG UACA-3′), RAD52 (5′-AGACU ACCUG AGAUC ACUAtt-3′), POLD3 (5′-GGCCU CUGUU CAAUA CUGAtt-3′), RAD18 (5′-GCUCU CUGAU CGUGA UUUA-3′), USP1 (5′-AGCUA CAAGU GAUAC AUUAtt-3′), SLX4 5′ UTR [SLX4 UTR87 (5′-GCACC AGGUU CAUAU GUAUtt-3′)], SLX4 3′ UTR [SLX4 UTR7062 (5′-GCACA AGGGC CCAGA ACAAtt-3′)], SLX1 (5′-UGGAC AGACC UGCUG GAGAU Utt-3′), MUS81 (5′-UAGGA UCUUA GCUUC CUUCC CGCUGtt-3′), XPF (5′-GUAGG AUACU UGUGG UUGAtt-3′) and control siRNA (Bioneer #SN-1002). RNF168 siRNA (5′-GACAC UUUCU CCACA GAUAU U-3′) was purchased from GENOLUTION. SLX4 5′ UTR- and 3′ UTR-targeting siRNAs were used as a mixture.

Chemicals, reagents and antibodies

The following chemicals were used in this study: indole-3-acetic acid (IAA, auxin) (87, 51, 4) (Millipore); 4-hydroxytamoxifen (4-OHT, tamoxifen) (H7904), aphidicolin (A0781), thymidine (T1895), RO-3306 (SML0569, a cycle-dependent kinase (CDK)1 inhibitor), 5-ethynyl-2′-deoxyuridine (EdU) (#900 584), 5-bromo-2′-deoxyuridine (BrdU) (B5002), doxycycline hyclate (doxycycline) (D9891) (Sigma-Aldrich); 5-bromo-2′-deoxycytidine hydrate (BrdC) (#0 210 016 680), 5-chloro-2′-deoxyuridine (CldU) (#105 478) (MP Biomedicals); Shield1 (632 189) (TAKARA); colcemid (15212–012) (Gibco); ML323 (S7529, an USP1-UAF1 inhibitor, 30 μM), JH-RE-06 (S8850, a REV1 inhibitor, 2.5 μM), NSC697923 (S7142, UBE2N-UEV1A inhibitor, 10 μM), pyridostatin (PDS) (S7444, G4 stabilizer, 10 μM) (Selleckchem). The following reagents were used in this study: Hoechst 33 258 (H1398), Ultrapure 20X SSC (#15 557 044) (Invitrogen); DIG Easy Hyb solution (#11 603 558 001), Ponceau S solution (P7170) (Sigma-Aldrich); Exonuclease III (M1815), Set of each dNTPs (U1130) (Promega); formaldehyde (P2031), formamide (FC1014) (Biosesang). The following antibodies were used: anti-UAF1 (sc-514473), anti-GFP (sc-8334), anti-RAD52 (sc-365341), anti-PML (sc-966), anti-Lamin B1 (sc-20682) (Santa Cruz Biotechnology); rabbit-anti-PCNA (ab18197), anti-RAD18 (ab57447), horseradish peroxidase (HRP)-conjugated anti-Digoxigenin (HRP.21H8) (ab6212), anti-FANCD2 (ab2187) for immunoblotting, anti-FANCD2 (ab108928) for immunostaining, anti-SLX4 (ab169114) for immunoblotting, anti-MUS81 (ab14387), anti-CldU (ab6326) (Abcam); anti-FLAG (F7425), anti-ssDNA (MAB3034) (Sigma-Aldrich); anti-ubiquityl-PCNA (Lys164) (13439S), anti-Cyclin B1 (4138S), anti-histone H3 (#9175) (Cell signaling); anti-γH2AX (05–636) (Merck Millipore); anti-POLD3 (H00010714-M01) (Abnova); anti-USP1 (A301-698A), anti-PML (A301-167A) for immunostaining (Bethyl); anti-ATRX (GTX101310) (GeneTex); anti-XPF (NBP2-58407) (Novus Biologicals); anti-SLX4 (DU16029) (MRC laboratory for immunostaining) antibodies. The anti-human ATAD5 antibody was raised in rabbits against an N-terminal fragment (1–297 aa) (35).

Flow cytometry and fluorescence *in situ* hybridization (Flow-FISH)

Flow-FISH assay to measure the average length of telomeres was performed as previously described (49) with slight modification. After trypsinization, 5×10^6 cells were collected and incubated with hybridization buffer (70% formamide, 20 mM Tris-HCl, pH 6.8, and 1% BSA in 2X SSC) at room temperature for 10 min. For probe denaturation, 0.05 μg/ml PNA probe (TelC-FITC) was added to the hybridization buffer and denatured at 82°C for 5 min, and rapidly cooled in ice for 2 min. After incubation with a denatured probe for 2 h at room temperature in dark, cells were washed with washing buffer (70% formamide, 10 mM Tris-HCl, pH 6.8, 0.1% BSA in TDW, and 0.1% Tween-20 in 2X SSC) twice. After centrifugation, pellets were subjected to propidium iodide staining (0.1% BSA, 10 mg/ml RNase A, 0.1 mg/ml propidium iodide) for overnight at 4°C in dark. Flow cytometry was performed on a FACSVerse™ flow cytometer using the BD FACSuite™ software (BD Biosciences). Each experiment began with calibration beads with Quantum™ FITC-5 MESF kits (#555p, Bangs Laboratories). Quantification and analysis were performed by using the QuickCal® v.3.0. software (Bangs Laboratories).

Southern blot analysis of terminal restriction fragment

TRF analysis was conducted to measure telomere length as previously described (50). Genomic DNA was extracted usingphenol/chloroform/isoamyl alcohol (25:24:1) solution, and its concentration and purity were measured. Purity was confirmed by an OD260/OD280 ratio between 1.6 and 1.9. Average telomere length was measured using the TeloTAGGG™ Telomere Length Assay Kit (Sigma-Aldrich) according to the manufacturer's instructions with slight modifications. A total of 10 μg of genomic DNA was digested overnight at 37°C with Hinf-I (New England Biolabs, R0155S) and Rsa-I (New England Biolabs, R0167S). For pulsed-field gel electrophoresis, the digested DNA was separated using the CHEF-DRII system (Bio-Rad). Samples were loaded into a 1% (wt/vol) PFGE-Certified™ agarose gel (#162–0138, Bio-Rad) in 0.5x TBE buffer under the following conditions: 6 V/cm, initial and final switch times ramped from 1-5 s, and an angle of ± 60° for 18 h at 14°C. The gel was stained with GelRed® nucleic acid gel stain (#41 003, Biotium) for 1 h at room temperature with shaking to visualize the restricted DNA. After staining, the gel was washed with DEPC-treated water and depurinated with 0.25 M HCl for 30 min. DNA in the gel was denatured (0.5 M NaOH, 1.5 M NaCl) and then neutralized (0.5 M Tris-HCl pH 7.5, 1.5 M NaCl) for 30 min each. The DNA was transferred to a Hybond N + membrane (RPN2020B, Amersham) using 10x SSC as the transfer buffer, following conventional Southern blotting methods, overnight. The Hybond N + membrane was crosslinked with 1200 J/m^2 UV (254 nm) twice, followed by incubation with a Digoxigenin (DIG)-labeled $(CCCTAA)_4$ probe in DIG Easy Hyb solution (Sigma-Aldrich) at a final concentration of 100 ng/ml with gentle agitation at 42°C overnight. The membrane was then washed, blocked, and subjected to an alkaline phosphatase-conjugated anti-DIG antibody for 1 h. Subsequently, the membrane was washed and incubated in detection solution for 5 min. The telomere band was detected using the DIG luminescent detection (DSP-Star) system and an automated imaging system (ChemiDoc™; Bio-Rad Laboratories).

Telomere fluorescence *in situ* hybridization (Telomere FISH)

Telomere FISH was performed after immunostaining and/or EdU-Click reaction. The cells in the slide were blocked by blocking solution (3% BSA in PBST). Cells were then fixed with 4% PFA for 10 min, dehydrated by sequential incubation in 75%, 85% and 100% ethanol for 2 min each, and allowed to air dry completely. For probe denaturation, hybridizing solution (70% formamide, 12 mM Tris-pH 7.5, 5 mM KCl, 1 mM $MgCl_2$ in 2X SSC) with 8 μg/ml peptide nucleic acid (PNA) probes TelC (repeats of CCCTAA)-Cy3 (F1002, Panagene) or TelG (repeats of TTAGGG)-FITC (F1010, Panagene) was preheated to 72°C for 5 min and immediately cooled at 4°C for 5 min. Air-dried cells were incubated in warmed 70% formamide solution in 2X SSC at 68°C for 5 min to denature genomic DNA. Cells were then incubated with hybridizing solution containing denatured telomere probes at 37°C for 2 h in the dark. Cells were washed at room temperature with 50%

formamide solution for 15 min, 2X SSC buffer and 0.1% NP-40 in 2X SSC solution.

Single-molecule analysis of telomeric DNA (SMAT) assay

Single-molecule analysis of telomeric (SMAT) assay was performed as previously described (51) with slight modification. Briefly, cells were labeled with 100 μM CIdU for 4 h before harvest. Cells were embedded in 1.2% low-melting agarose (#1 613 112, Bio-Rad) plugs and then subjected to digestion with MboI restriction enzyme (R0147M, NEB) and proteinase K (#3 115 828 001, Roche) overnight. Plugs were then dissolved with β-Agarase I (M0392S, NEB). Molecular combing was performed using the Molecular Combing System (Genomic Vision) with a constant stretch factor of 2 kb/μm using vinyl silane coverslips. Coverslips were then dried for 4 h at 65°C, and DNA was denatured in 2.5 M HCl for 1 h. DNA was then subjected to immunostaining for CldU and anti-ssDNA (MAB3034, Sigma-Aldrich) and followed telomere FISH with TelG-Cy3 probe (F1006, Panagene). The fiber images were acquired using a motorized fluorescence microscope (Axio Observer 7, Carl Zeiss) with 0.1 μm resolution grid projection with 60×/oil 27 μm objective. Fibers were quantified from individual tiles with Zen 2.6 (blue edition) (Carl Zeiss) software. More than 350 fibers were counted for each replicate in each experiments.

Chromosome orientation-FISH (CO-FISH)

CO-FISH assay to detect T-SCE was performed as previously described (52) with slight modification. Cells were incubated with 10 μM of BrdU:BrdC (3:1) for 24 h, for 18 h in the case of the GM0637 cell line, before fixation. For removal of BrdU- and BrdC-incorporated (newly synthesized) DNA strand, the slide was incubated in RNase A (100 μg/ml) at 37°C for 10 min. DNA was then stained with Hoechst 33 258 (500 μg/ml) in 2X SSC at room temperature for 15 min followed by a rinse with triple distilled water (TDW) and air dry. The slide was exposed to 365 nm ultraviolet light for 30 min and incubated with Exonuclease III solution (10 U/μl) at room temperature for 30 min. Telomere FISH was performed twice in a row by using TelG-FITC and TelC-Cy3 probes.

C-circle amplification assay

The C-circle assay was performed as previously described (53) with slight modification. To isolate genomic DNA, cell pellets were resuspended with QCP lysis buffer [50 mM KCl, 10 mM Tris-HCl, pH 8.5, 2 mM $MgCl_2$, 0.5% IGEPAL CA-630 (I8896, Sigma), 0.5% Tween-20 in DEPC-treated TDW with protease (#19 155, QIAGEN), 0.053 AU/ml], and incubated with a shake at 1400 rpm at 56°C for 1 h. To inactivate the protease activity, lysed cells were subjected to heat treatment at 70°C for 20 min. For C-circle amplification, 10 μl of 0.1–1 μg genomic DNA was mixed with 10 μl of 2X C-circle master mix [0.2 mg/ml BSA (NEB), 0.2% Tween-20, 2 mM dATP, 2 mM dGTP, 2 mM dTTP, 8 mM DTT, 2X ϕ29 buffer in DEPC-treated TDW] supplemented with ϕ29 polymerase (EP0091, Thermo Scientific) or DEPC-treated TDW. C-circle amplification was performed at 30°C for 8 h, followed by ϕ29 polymerase heat inactivation at 65°C for 20 min and cooling at 4°C using PCR thermocycler (Eppendorf). Amplified C-circle DNA was diluted with 2X SSC buffer and loaded onto a dot-blot apparatus bedded with Hybond N + membrane (RPN2020B, Amersharm). Bounded DNA was crosslinked to the membrane by exposing the membrane to 1300 J/m^2 UV (254 nm) using a UV crosslinker (Stratagene). The membrane was pre-hybridized with DIG Easy Hyb solution (Sigma-Aldrich) at 42°C for 1 h. Digoxigenin-labeled oligonucleotide probes $(CCCTAA)_4$ were added to the DIG Easy Hyb solution at a final concentration of 100 ng/ml and incubated with gentle agitation at 42°C overnight. The membrane was sequentially washed with 0.1% SDS in 2X SSC at room temperature and 0.1% SDS in 0.2X SSC at 50°C for 20 min each with gentle agitation. The membrane was then incubated with HRP-conjugated anti-Digoxigenin-antibody for 6 h. After washing with TBST buffer, the signal was detected using enhanced a chemiluminescence reagent (Thermo Fisher Scientific) with an automated imaging system (ChemiDoc™; Bio-Rad Laboratories).

Chromatin immunoprecipitation (ChIP) and dot blot

ChIP was performed using SimpleChIP® Enzymatic Chromatin IP Kit (#9002, Cell Signaling Technology) according to the manufacturer's instructions. U2OS-ATAD5^{AID} cells were arrested at G2 phase as described, and then cross-linked with 1% (v/v) formaldehyde for 10 min, and then glycine was added to 125 mM for 5 min to stop the cross-linking at room temperature. After 1X phosphate-buffered saline (PBS) washing, cells were collected with 100 mM phenylmethylsulfonyl fluoride (PMSF), phosphatase inhibitors and protease inhibitors. Cells were then lysed, and nuclei were isolated. The cross-linked chromatin was sonicated to a length of 150–500 bp with a high-performance sample (DNA) preparation ultrasonicator at 4°C (Duty 10, PIP 175, Cycle 200) (Covaris-S220, Covaris®), and then centrifugation with 9400 *g* for 10 min at 4°C. An aliquot of each ChIP sample was prepared as input control, while the rest of the DNA was incubated with 5 μg of either anti-PCNA (ab18971, Abcam) or anti-IgG (P120-301, Bethyl Lab) antibody as negative control overnight at 4°C. After adding ChIP-grade protein G agarose beads for 2 h at 4°C, chromatin complex was washed by low- and high-salt ChIP buffer, and de-crosslinked by NaCl, RNase A and proteinase K at 65°C for 2 h. Eluted DNA was then cleaned with DNA purification spin columns and processed for dot blot analysis of telomere content described in C-circle method section.

ALT telomere DNA synthesis in APBs (ATSA) assay

ALT telomere DNA synthesis in APBs (ATSA) assay was performed as previously described (7) with slight modification. To synchronize cells in the G2 phase, cells were treated with 2.5 mM thymidine for 20 h, released into a fresh medium for 6 h, and then treated with 15 μM RO-3306 (CDK1i) for 16 h before fixation. The synchronization was confirmed by flow cytometry analysis of cells additionally labeled with 10 μM EdU for 30 min. For visualization of DNA synthesis in APBs, cells were incubated with 20 μM EdU for 30 min before fixation. The fixed cells were subjected to immunostaining for PML, EdU-click reaction, and followed telomere FISH with TelC-Cy3 probe.

Mitotic DNA synthesis (MiDAS) assay

MiDAS assay was performed as previously described (54) with slight modification. After transfection, cells were treated with 0.4 μM aphidicolin for 16 h and 15 μM of RO-3306 (CDK1i) for 6 h before colcemid treatment. After washing with 1X

PBS, cells were incubated in fresh culture media (to release cells from G2 arrest) containing 1X colcemid (to arrest cells at the metaphase) and 20 μM EdU (to label MiDAS) for 1 h before fixation. After trypsinization, cells were slowly mixed with pre-warmed 75 mM KCl in a drop-wise manner and then incubated at 37°C for 12 min. Cells were then fixed using a cold fixative solution (methanol/acetic acid 3:1). After fixation, cells in suspension were spread onto a clean slide and exposed to 90°C steam for 30 s. Slides were dried at room temperature for 1 h. Cells were then subjected to EdU-click reaction and followed telomere FISH with TelC-Cy3 probe.

EdU-click chemistry for ATSA, MiDAS, and cell cycle analysis

Cells were labeled with 10–20 μM EdU according to conditions in each assay. After EdU labeling, a click reaction was performed using the Click-iT® EdU Imaging kit (Thermo Fisher Scientific), according to the manufacturer's instructions. For EdU-click reaction for MiDAS assay, cells were incubated with pre-extraction buffer (descripted in immunostaining section) for 10 min at 4°C. Cells were then rinsed with 1X cold-PBS, fixed with 4% PFA for 15 min, and permeabilized with 0.5% Triton X-100 for 5 min before click-reaction. For cell cycle analysis, cells were labeled with 10 μM EdU for 30 min before harvesting and processed using the Click-iT® EdU flow cytometry assay kit (C10643) (Thermo Fisher). In brief, cells were fixed, permeabilized and subjected to click reaction. Cells were then incubated in PBS with 0.1 mg/ml RNase A for 1 h at 37°C and DNA was stained with 0.05 mg/ml propidium iodide. Flow cytometry was performed on a FACSVerse™ flow cytometer using the BD FACSuite™ software (BD Biosciences). Data analysis was performed by using the FlowJo software.

TRF1-FokI-induced generation of telomeric breaks in the G2 phase

To generate telomeric breaks in U2OS-mCherry-TRF1-FokI cells in the G2 phase, cells were simultaneously treated with 100 ng/ml doxycycline (induces expression of DD-ER-mCherry-TRF1-FokI proteins) and 15 μM RO-3306 (arrests cells in the G2 phase) for 16 h, and then treated with 1 μM tamoxifen (binds to ER and induces nuclear transport of proteins fused to ER) and 1 μM Shield1 (stabilizes proteins tagged with a DD domain) for 2 h, otherwise descripted in the figure legends. To detect break-induced telomere synthesis (EdU localization at TRF1-FokI), 10 μM EdU was added to cells before 10 min fixation.

Immunostaining

Immunostaining with the metaphase spread was performed as previously described (36) with slight modification. After trypsinization, cells were incubated with hypotonic solution (75 mM KCl) and fixed with fixative solution (methanol/acetic acid 3:1). Fixed cells were spread onto a slide and incubated with pre-extraction buffer (0.1% Triton X-100, 20 mM HEPES-KOH, pH 7.9, 50 mM NaCl, 3 mM $MgCl_2$, 300 mM sucrose) for 10 min at 4°C. The slide was then rinsed with 1X cold PBS, and cells were fixed with 4% paraformaldehyde (PFA) for 15 min and permeabilized with 0.5% Triton X-100 in PBS for 5 min. Cells were then blocked with blocking buffer [5% bovine serum albumin (BSA) and 0.5% Triton X-100 in PBS] for 1 h and incubated with the primary antibody in blocking solution overnight at 4°C. After washing with the wash buffer (0.1% Triton X-100 in PBS), cells were incubated with Alexa Fluor-conjugated secondary antibody (1:500) in wash buffer for 1 h at room temperature. After washing with washing buffer, the cells were mounted using ProLong® Gold antifade reagent with DAPI (H-1200) (Vector Laboratories) or proceeded for further assays.

Image acquisition and image analysis

For all immunostaining assays combined with telomere FISH (except PCNA) or EdU-Click reaction, including ATSA, MiDAS, SMAT assay and CO-FISH assay, images were acquired using a BX53 fluorescence microscope (Olympus LS) with cellSens v.1.18 imaging software and analyzed with OlyVIA software (Olympus LS). For PCNA immunostaining with telomere FISH, confocal images were acquired using an LSM880 confocal microscope (Carl Zeiss) with a 40×/1.2 lens objective. Image acquisition and analysis were performed with Zen 2.6 (blue edition) (Carl Zeiss) software.

Protein extraction and immunoblot analysis

Protein extraction and immunoblot analysis were performed as previously described (36). For whole-cell proteins extraction, cell pellets were lysed in radioimmunoprecipitation assay (RIPA) buffer (50 mM Tris-HCl, pH 8.0, 150 mM NaCl, 5 mM EDTA, 1% Triton X-100, 0.1% sodium dodecyl sulfate, 0.5% sodium deoxycholate, 0.1 M phenylmethylsulfonyl fluoride, phosphatase inhibitors and protease inhibitors) with Benzonase nuclease for 45 min at 4°C, followed by sonication and centrifugation. For chromatin-bound protein extraction, cell pellets were first resuspended in Buffer A (100 mM NaCl, 300 mM sucrose, 3 mM $MgCl_2$, 10 mM piperazine-N,N'-bis(2-ethanesulfonic acid) (PIPES), pH 6.8, 1 mM ethylene-bis(oxyethylenenitrilo)tetraacetic acid (EGTA), 0.2% Triton X-100, 0.1 M phenylmethylsulfonyl fluoride, phosphatase inhibitors and protease inhibitors) and incubated for 5 min at 4°C. After centrifugation, pellets were further lysed in RIPA buffer. For immunoblot analysis, proteins were separated by SDS-PAGE and transferred to a nitrocellulose membrane. The blot was blocked with Tris-buffered saline containing 0.1% Tween 20 (TBST) supplemented with 5% skim milk for 30 min and incubated with primary antibodies overnight. After washing with TBST buffer, the blot was incubated with HRP-conjugated secondary antibodies (Enzo Life Sciences) for 30 min. After washing with TBST buffer, the signal was detected using an enhanced chemiluminescence reagent (Thermo Fisher Scientific) with an automated imaging system (ChemiDoc™; Bio-Rad Laboratories).

Reverse transcription-quantitative real-time PCR (RT-qPCR)

Total RNA was extracted using a TRIzol® Reagent (Invitrogen) protocol. 1.5 μg RNA was used to synthesize cDNA using the SuperScript® IV First-Strand Synthesis System (18 091 050) (Invitrogen). RT-qPCR was performed using Power SYBR Green master mix (4 368 702) (Applied Biosystems) in a QuantStudio 7 Flex system (Applied Biosystems) according to the manufacturer's instructions. Gene expression was normalized to *36B4* expression. The following primers were used: 36B4U-forward (For) (5′-CAGCA AGTGG GAAGG TGTAA TCC-3′), 36B4D-reverse (Rev) (5′-CCCAT TCTAT CATCA ACGGG TACAA-3′),

RNF168-For (5′-GGCGA GTTTA TGCTG TCCCT-3′), RNF168-Rev (5′-GCCGC CACCT TGCTT ATTTC-3′), SLX1-For (5′-ATGCC CTTGC TGTGA GAAGT-3′), SLX1-Rev (5′-GGTAG GAGGG GGTAA GGACA-3′).

Statistical analysis

Prism 9 (GraphPad Software) was used to generate graphs and analyze data. Error bars represent the standard deviation (s.d.) of the mean (mean ± s.d.). For statistics, we used one-way ANOVA, along with a post-hoc Tukey test or two-tailed unpaired Student's *t*-test, as descripted in the figure legends; $****P<0.0001$, $***P<0.001$, $**P<0.01$, $*P<0.05$ and n.s.: not significant. Statistical parameters are described in the figures.

Results

Ub-PCNA localization at APBs increases in ATAD5-depleted cells in the G2 phase

PCNA localizes at APBs and participates in telomeric DNA synthesis (55). RAD18, a PCNA ubiquitinating enzyme (Figure 1A), also colocalizes with APBs (56). Because ATAD5 participates in PCNA unloading and deubiquitination at replication forks or DNA damage sites (Figure 1A) and APBs are enriched in the G2 phase of the cell cycle (57), we examined the effects of ATAD5 depletion on PCNA and Ub-PCNA levels at telomeres in the G2 phase using ALT + U2OS cancer cell line with endogenous ATAD5 protein fused to an auxin-inducible degron (AID) (Supplementary Figure S1A) (38). We found that PCNA was enriched at telomeric DNA in the G2 phase, and the level of enrichment was increased when ATAD5 was degraded by the auxin treatment (Supplementary Figure S1B and C). More importantly, both PCNA and Ub-PCNA localized at APBs in the G2 phase and that the level of localization was increased after ATAD5 depletion (Figure 1B–E), suggesting that PCNA and Ub-PCNA remain at APBs in ATAD5-depleted cells.

Ub-PCNA increases APBs with DNA synthesis in the G2 phase

Next, we analyzed the effects of ATAD5 depletion on telomeric DNA synthesis by using the ALT telomere DNA synthesis in APBs (ATSA) assay that detects intact telomere extension in ALT + cells in the G2 phase (7). As previously reported, EdU foci were detected in a fraction of APBs of most U2OS cells in the G2 phase (Figure 1F, Supplementary Figure S1D and E). ATAD5 depletion increased the number of total APBs and EdU^+ APBs (Figure 1F–H). Consistent with the cooperative role of ATAD5 and USP1 in PCNA deubiquitination (Figure 1A) (35), USP1 depletion also increased the number of total APBs and EdU^+ APBs, which was reduced when RAD18 was co-depleted (Figure 1I,J and Supplementary Figure S1F). We found that RAD18 depletion alone decreased the number of total APBs and EdU^+ APBs (Figure 1I and J), which appears to contradict an increase in the percentage of APB-positive cells by RAD18 depletion in asynchronous U2OS cells (56). No discernible difference in the cell cycle after RAD18 depletion (Supplementary Figure S1G–I), excluding the effect of the G2 population. We found an increase in cells with low numbers of APBs following RAD18 depletion in asynchronous U2OS cells (Supplementary Figure S1J), which could lead to an overall reduction in the number of APBs per cell (Supplementary Figure S1K). Collectively, these results suggest that APB formation and telomeric DNA synthesis are restricted by PCNA deubiquitination.

Ub-PCNA increases BIR-like mitotic DNA synthesis events in ALT + cancer cells

ALT-mediated telomeric DNA synthesis occurs via a BIR-like process (6,7,47). Therefore, we investigated BIR-mediated MiDAS at telomeres and CFSs in the three ALT + cell lines, U2OS, GM0637 and SK-LU-1 (Figure 2A and Supplementary Figure S2A–D) (8,19,20,58). ATAD5 depletion increased MiDAS events at both telomeres and CFSs in U2OS cells under replication stress (Figure 2B,C). Similar increases in MiDAS events at telomeres were observed in GM0637 and SK-LU-1 cells upon ATAD5 depletion (Figure 2D,E). Co-depletion of POLD3 or RAD52 with ATAD5 restored MiDAS events to baseline levels in U2OS cells (Figure 2F,G and Supplementary Figure S2E,F), suggesting the observed MiDAS occurs via a BIR-like process. The dependence of this process on RAD52 was confirmed using $RAD52^{-/-}$ U2OS cells in which RAD52 expression can be induced by doxycycline (7) (Figure 2H and Supplementary Figure S2G). Interestingly, ATAD5 depletion did not increase MiDAS at CFSs or telomeres in TEL + HeLa_long telomere (HeLa_LT) cells (Figure 2I,J and Supplementary Figure S2H).

Consistent with the ATSA results, RAD18 depletion reduced the telomeric MiDAS induced by ATAD5 depletion in U2OS cells (Figure 2K and Supplementary Figure S2I). In contrast, USP1 depletion increased telomeric MiDAS to the level caused by ATAD5 single depletion, and this effect was not further increased by ATAD5 co-depletion (Figure 2L and Supplementary Figure S2J) but was restored to basal levels when either RAD18 or RAD52 was co-depleted (Figure 2M,N and Supplementary Figure S2K). MiDAS at CFSs was also similarly regulated by USP1 or RAD18 in U2OS cells (Figure 2O). In contrast, MiDAS levels at telomeres and CFSs in HeLa_LT cells were not affected by USP1 or RAD18 depletion (Figure 2P,Q and Supplementary Figure S2L). Considering that MiDAS in ALT + and TEL + cells share nearly the same BIR process (20,58), these results collectively suggest that unprocessed Ub-PCNA increases BIR events only in ALT + cancer cells.

Ub-PCNA increases break-induced telomere synthesis

The telomeric repeat binding factor 1 (TRF1)-FokI endonuclease inducible cell system has been used to study double-strand break (DSB)-induced telomere synthesis (Figure 3A) (47). TRF1-FokI-induced telomere synthesis occurs in both ALT + and TEL + cells and the synthesis depends on PCNA and POLD3 (47,59). Upon induction of nuclear localization of the TRF1-FokI protein by tamoxifen treatment in the G2 phase, PCNA and EdU foci were colocalized with TRF1-FokI foci (Supplementary Figure S3A), as reported (47). Ub-PCNA also colocalized with TRF1-FokI and EdU foci upon inducing telomere breaks (Figure 3B), which was significantly reduced by RAD18 depletion (Figure 3C,D). Residual localization of Ub-PCNA at telomeric breaks might be explained by siRNA efficiency but not by RNF168-mediated PCNA ubiquitination (60), because the percent localization was not affected by RNF168 depletion (Supplementary Figure S3B,C). We found that EdU signal at TRF1-FokI foci, which indicates

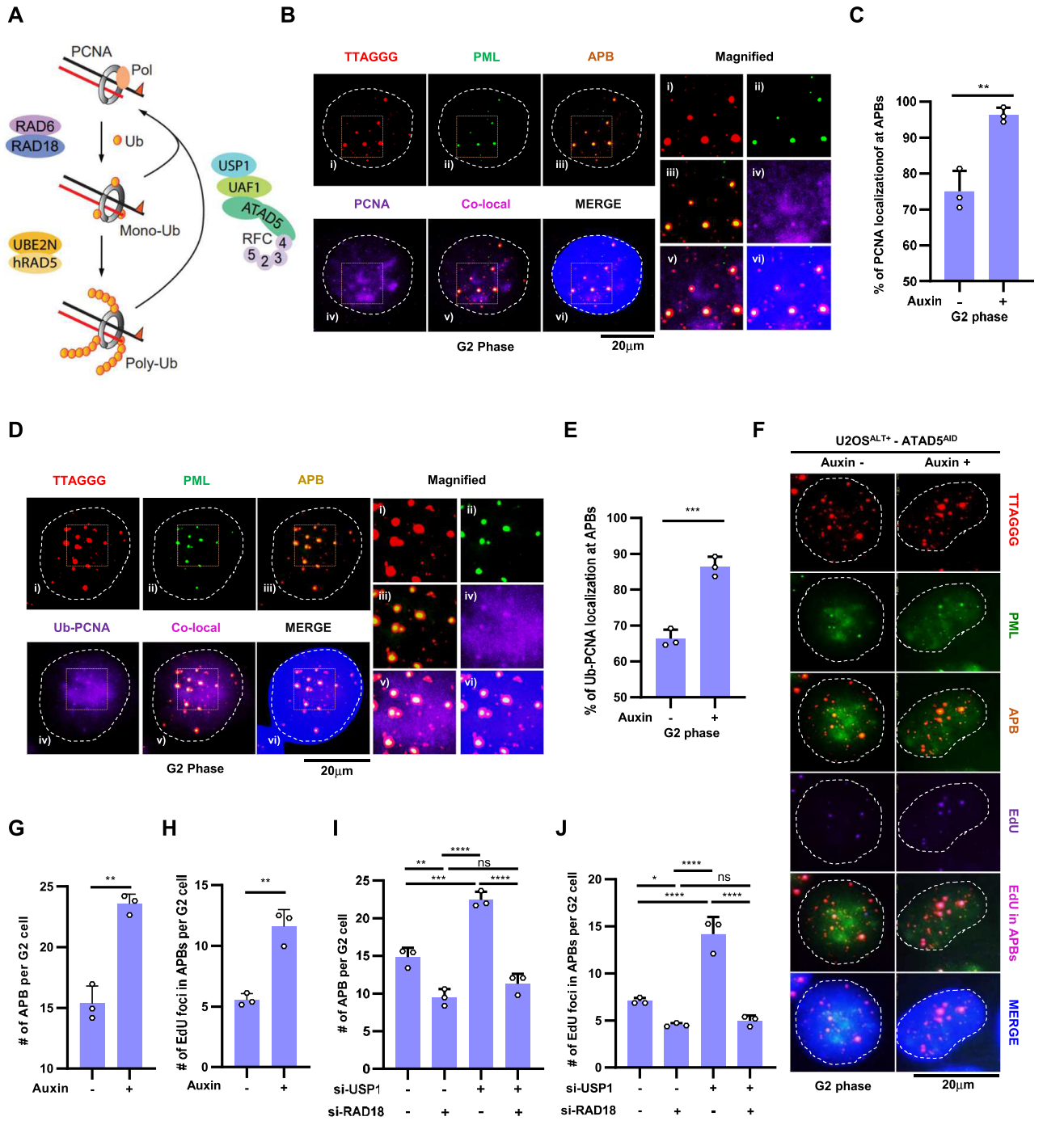

Figure 1. Ub-PCNA increases APBs with DNA synthesis in the G2 phase of ALT + cancer cells. (**A**) A diagram of PCNA ubiquitination and de-ubiquitination. The triangle on the DNA represents a DNA lesion. (**B–E**) U2OS-ATAD5^{AID} cells were treated with auxin for 48 h and fixed at the G2 phase for immunostaining with telomere FISH. (B,D) Representative images of localization of PCNA (B) or Ub-PCNA (D) at APBs. (C,E) The percent localization of PCNA (C) or Ub-PCNA (E) at APBs per G2 phase cell was quantified. (**F–H**) U2OS-ATAD5^{AID} cells were treated with auxin for 48 h and fixed at the G2 phase for an ATSA assay. (**I,J**) After siRNA transfection, G2-synchronized U2OS cells were subjected to an ATSA assay. (G–J) Quantification ATSA results were displayed. (B,D,F) The dotted line represents the edge of the nucleus. Data in all graphs represent the mean ± s.d. of at least three independent experiments. Statistical analysis: two-tailed unpaired Student's *t*-test (C, E, G, H); one-way ANOVA (I,J). ****P<0.0001, ***P<0.001, **P<0.01, *P<0.05 and ns.: not significant.

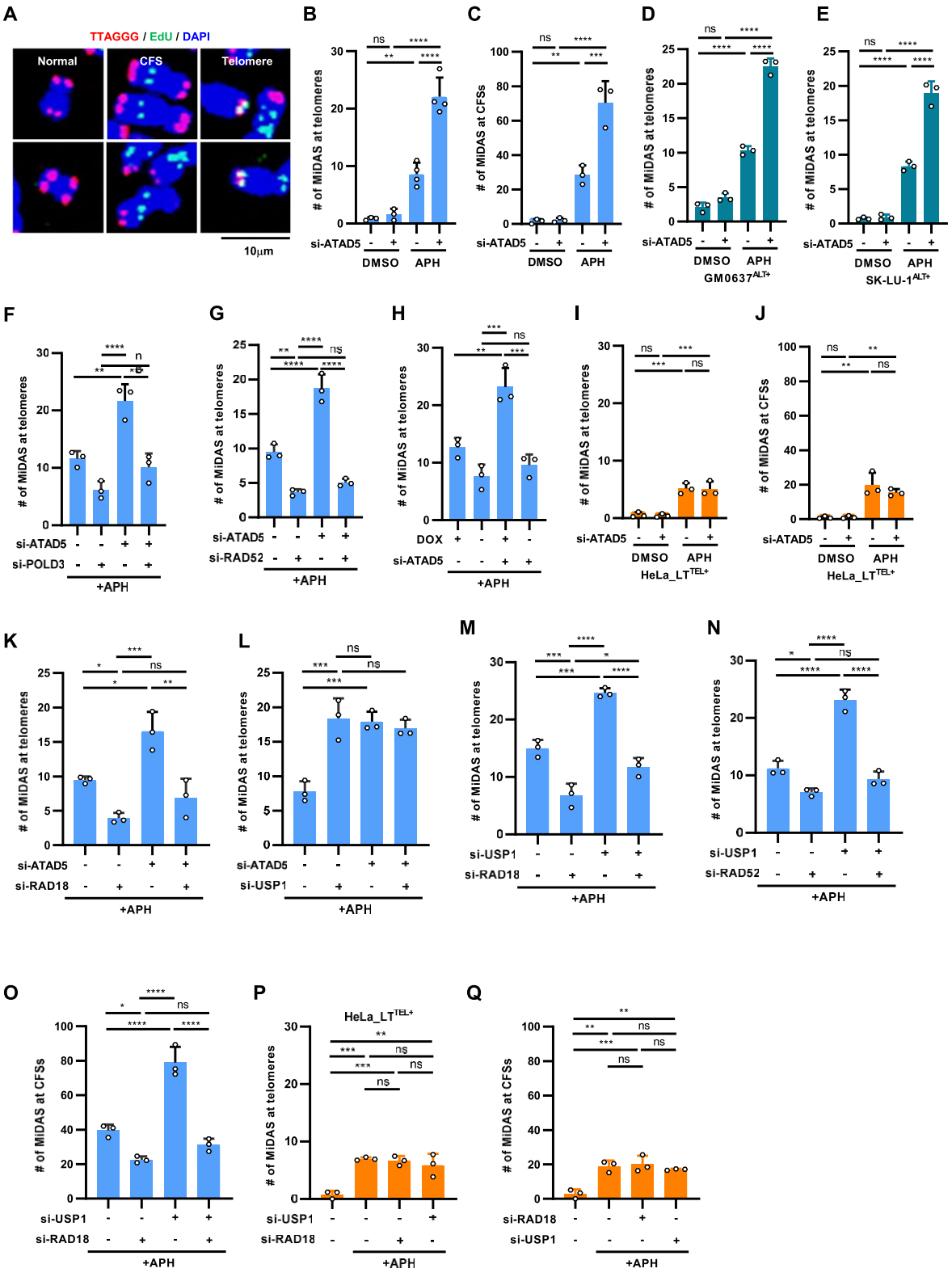

Figure 2. Ub-PCNA increases BIR-like MiDAS events in ALT + cancer cells. (A) Representative images of MiDAS after APH treatment. (**A–Q**) After transfection, cells were treated with DMSO or 0.4 mM aphidicolin (APH) for 16 h and subjected to a MiDAS assay. (B–Q) The number of MiDAS at telomeres or CFS regions per metaphase cell was quantified. (H) RAD52 expression was induced by doxycycline (DOX) for 48 h. Cell lines: U2OS (B,C,F–H,K–O), GM0637 (D), SK-LU-1 (E), *RAD52*$^{-/-}$ U2OS (H) and HeLa_LT (I,J,P,Q). Data in all graphs represent the mean ± s.d. of at least three independent experiments. Statistical analysis: One-way ANOVA (B–Q). ****P<0.0001, ***P<0.001, **P<0.01, *P<0.05 and ns.: not significant.

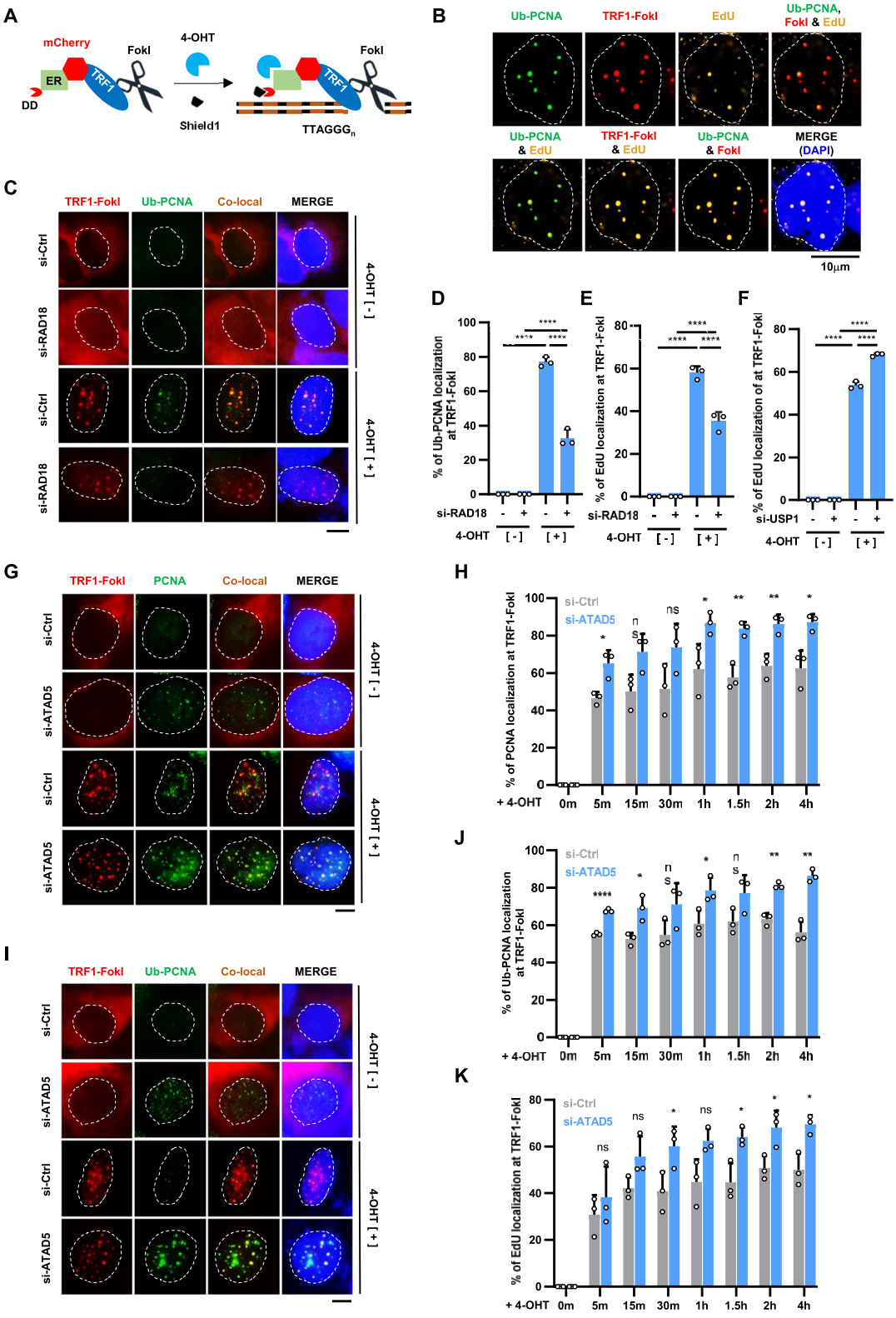

Figure 3. Ub-PCNA increases break-induced telomere synthesis. (**A**) A diagram of the TRF1-FokI system. (**B–K**) After siRNA transfection, U2OS-mCherry-TRF1-FokI cells were enriched in the G2 phase and treated with tamoxifen and Shield1 for 2 h (B–F,G,I) or indicated times (H,J,K) before fixation for immunostaining. (B) Representative immunostaining images of Ub-PCNA, EdU and TRF1-FokI co-localization after telomeric break induction. (C,G,I) Representative images showing localization of Ub-PCNA (C,I) or PCNA (G) at TRF1-FokI foci. Scale bar 10 μm. (D–F,H,J,K) The percent localization of Ub-PCNA (D,J), EdU (E,F,K) or PCNA (H) at TRF1-FokI foci was quantified. (B,C,G,I) The dotted line represents the edge of the nucleus. Data in all graphs represent the mean ± s.d. of at least three independent experiments. Statistical analysis: One-way ANOVA (D–F); two-tailed unpaired Student's *t*-test (H,J,K). ****P<0.0001, ***P<0.001, **P<0.01, *P<0.05 and ns.: not significant.

break-induced telomere synthesis, was reduced by RAD18 depletion and increased by USP1 depletion (Figure 3E,F).

PCNA and Ub-PCNA localization at TRF1-FokI foci was consistently increased in the G2 phase by ATAD5 depletion (Figure 3G–J and Supplementary Figure S3D–F). PCNA or Ub-PCNA signal was observed at TRF1-FokI foci starting at 5 min after break induction, and colocalization events were more frequent at all time points in ATAD5-depleted cells (Figure 3H,J and Supplementary Figure S3E and F). Similarly, EdU signal at TRF1-FokI foci was observed beginning at 5 min after break induction (Figure 3K), suggesting a rapid onset of telomere synthesis. ATAD5 depletion resulted in an increase in telomere synthesis events at all time points (Figure 3K). Taken together, these results suggest that PCNA ubiquitination contributes to break-induced telomere synthesis.

ATAD5 deficiency extends telomere length in ALT + cancer cells

ATAD5 depletion increased APBs with DNA synthesis and break-induced telomere synthesis, and *elg1Δ* mutants exhibit telomere elongation (41,42). We therefore investigated the effect of long-term ATAD5 depletion on telomere length using U2OS-and HeLa-ATAD5^{AID} cells. During 40 days of auxin treatment, depletion of endogenous ATAD5 and consequent increases in PCNA and monoUb-PCNA levels on chromatin were maintained in both cell lines (Supplementary Figure S4A). Flow-FISH to measure the average length of telomeres showed that telomere lengthening started to appear in U2OS-ATAD5^{AID} cells treated with auxin for just 10 days (Figure 4A). However, auxin treatment even for 40 days did not change the telomere length in HeLa-ATAD5^{AID} cells (Figure 4B). In addition, *ATAD5*$^{-/-}$ U2OS and other ALT + *ATAD5*$^{-/-}$ SK-LU-1 clones, but not TEL + *ATAD5*$^{-/-}$ HeLa_LT clones, showed telomere lengthening (Figure 4C and Supplementary Figure S4B). Analysis of terminal restriction fragments also showed telomere lengthening in *ATAD5*$^{-/-}$ U2OS, but not in *ATAD5*$^{-/-}$ HeLa_LT cells (Figure 4D). In addition, we examined telomeric DNA extension using a single-molecule analysis of telomeres (SMAT) assay (61). The length and the number of events of telomeric extension, which was marked by the incorporation of the thymidine analog 5-chloro-2′-deoxyuridine strictly at one end of the telomere, were increased in U2OS cells upon ATAD5 depletion (Figure 4E–G). Taken together, these results suggest that ATAD5 depletion leads to telomere lengthening in ALT + cancer cells.

Ub-PCNA promotes recombination-associated ALT phenotypes

Telomeric DNA synthesis in APBs and MiDAS, both of which were increased upon ATAD5 depletion, involves a recombination process (7,8). Therefore, we investigated the effects of ATAD5 depletion on recombination-associated ALT phenotypes such as telomere-sister chromatid exchange (T-SCE) and C-circle, a type of extrachromosomal telomeric repeat that is a byproduct of telomere recombination in the ALT pathway (62). We found that ATAD5 depletion increased T-SCE and C-circle levels in three different ALT + cell lines, but not in TEL + HeLa-originated cells (Figure 4H–L and Supplementary Figure S4C–H). USP1 depletion also increased C-circle levels in U2OS cells (Figure 4M). Consistently, the increases in T-SCE and C-circle induced by ATAD5 depletion were not restored by the UAF1-interaction-deficient ATAD5 (ATAD5$^{\Delta UAF1}$), which is defective in USP1-mediated PCNA deubiquitination (35), in contrast to the recovery to basal levels by wild-type ATAD5 (Figure 4N,O and Supplementary Figure S4I). Interestingly, the PCNA-unloading-defective ATAD5 ATPase mutant (ATAD5^{E1173K}) showed similar defects (Figure 4N,O). Taken together, these results suggest that both the PCNA deubiquitination and unloading activity of ATAD5 are required to inhibit recombination-associated ALT phenotypes.

Unprocessed ub-PCNA during the G2 phase increases APBs

Telomeric replication stress leads to APB formation and telomeric DNA synthesis in ALT + cells (8,63). There is a possibility that ATAD5 or USP1 deficiency may have an effect on replication stress itself (39). Therefore, we investigated the effect of ATAD5 or USP1 deficiency on ALT after excluding its influence on replication stress during the S phase. For this purpose, G2-phase synchronized U2OS-ATAD5^{AID} cells were treated with auxin for 6 h to acutely degrade the ATAD5 protein or treated with ML323, a chemical inhibitor of USP1-UAF1 (hereafter referred to as USP1i) (64). Both treatments increased chromatin monoUb-PCNA and diUb-PCNA levels (Figure 5A). The effects of USP1i on Ub-PCNA were more pronounced in the G2 phase (Supplementary Figure S5A). Combining the two treatments further increased the levels of the monoUb- and diUb-PCNA (Figure 5A). This could be explained by the persistence of all PCNA species on the chromatin due to the loss of the PCNA unloading activity of the ATAD5-RLC (32).

We found that acute ATAD5 degradation during the G2 phase increased the number of total APBs and EdU + APBs (Figure 5B and C). G2-specific USP1i treatment also increased the APBs and EdU + APBs (Figure 5B-E), which was further increased by ATAD5 depletion (Figure 5B and C) but restored to basal levels when RAD18 was depleted (Figure 5D,E and Supplementary Figure S5B). This suggests that a substantial amount of Ub-PCNA is retained until the G2 phase to facilitate APB formation, which is promoted when Ub-PCNA is not deubiquitinated during the G2 phase.

Unprocessed ub-PCNA during the G2 phase induces telomere damage and APB formation in a RAD52-independent manner

Based on the increased number of APBs by USP1 inhibition, we speculated that the increase in Ub-PCNA levels may be involved in the generation of telomeric damage leading to APB formation. Therefore, we examined DNA damage foci at telomeres called telomere dysfunction-induced foci (TIFs) (65). The number of TIFs was increased in U2OS cells treated with USP1i in the G2 phase (Figure 5F–H). The number of APBs in the G2 phase was minimally affected by RAD52 or POLD3 depletion (7), suggesting that the clustering of damaged telomeres occurs before BIR initiation at APBs. Consistent with these results, there was no significant difference in TIFs induced by USP1i in wild type and *RAD52*$^{-/-}$ U2OS cells (Figure 5F–H). As previously reported (7), RAD52 deficiency completely inhibited DNA synthesis but did not affect total APB number (Figure 5I,J). Interestingly, increased APB formation induced by USP1i was not affected by RAD52 deficiency (Figure 5I,J). Taken together, these results suggest that

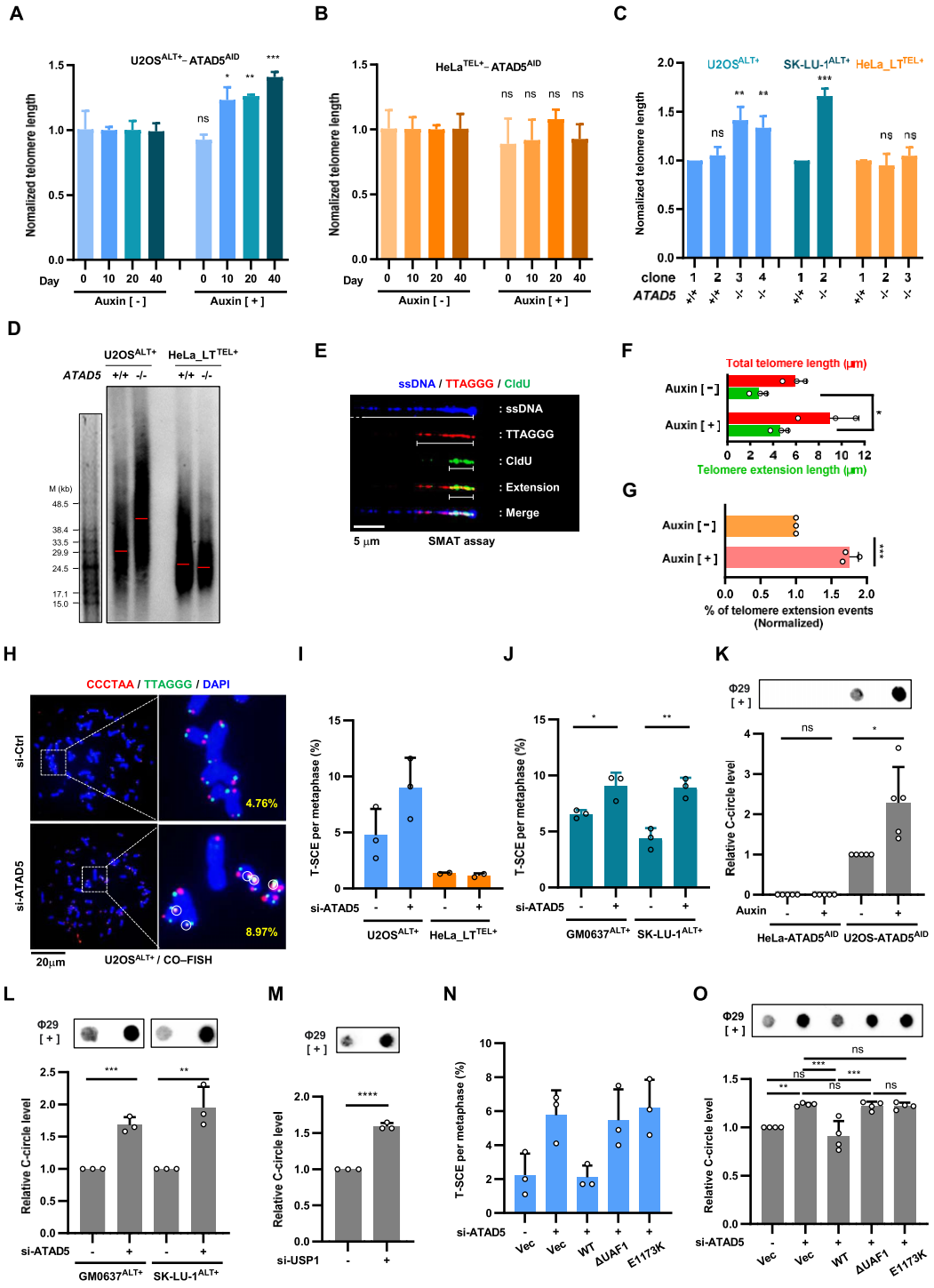

Figure 4. ATAD5 deficiency extends telomere length in ALT + cancer cells and promotes recombination-associated ALT phenotypes. (**A,B**) U2OS-ATAD5^{AID} or HeLa-ATAD5^{AID} cells were treated with auxin for the indicated days and subjected to a Flow-FISH assay. (**C**) *ATAD5*$^{+/+}$ and *ATAD5*$^{-/-}$ clones of each cell line were subjected to a Flow-FISH assay. (A–C) Normalized telomere length was quantified. (**D**) *ATAD5*$^{+/+}$ and ATAD5$^{-/-}$ U2OS and HeLa-LT cells were subjected to a terminal restriction fragment assay to measure actual telomere length. (**E–G**) U2OS-ATAD5^{AID} cells were treated with auxin and subjected to an SMAT assay. (E) Representative images of an SMAT assay. After the continuous long ssDNA fibers that were aligned with the telomere and CldU signal, and the terminal CldU signal was defined as telomere extension. (F,G) The total length of telomeres with the extension and extended telomere length (F), and the percentage of telomere extension events (G) were quantified from at least 350 fibers per each replicate. Data represent the mean ± s.d. of three independent experiments. (**H–J,L–O**) After transfection, cells were subjected to a CO-FISH to measure T-SCE (H–J, N) and C-circle assay (L,M,O). (H) Representative images of CO-FISH. A circle indicates a T-SCE event. (I,J,N) The percentage of T-SCE per metaphase was quantified. (**K**) U2OS-ATAD5^{AID} or HeLa-ATAD5^{AID} cells were treated with auxin for 48 h and subjected to a C-circle assay. (K,L,M,O) The intensity of the C-circle level was quantified. (N,O) U2OS cells were transfected with a combination of *ATAD5* siRNA and wild type (WT), UAF1 interaction-defective (ΔUAF1) or PCNA unloading-defective (E1173K) ATAD5 cDNA. Data in all graphs represent the mean ± s.d. of at least three independent experiments. Statistical analysis: two-tailed unpaired Student's *t*-test (A–C, F, G, J–M); One-way ANOVA (O). ****P<0.0001, ***P<0.001, **P<0.01, *P<0.05 and ns.: not significant.

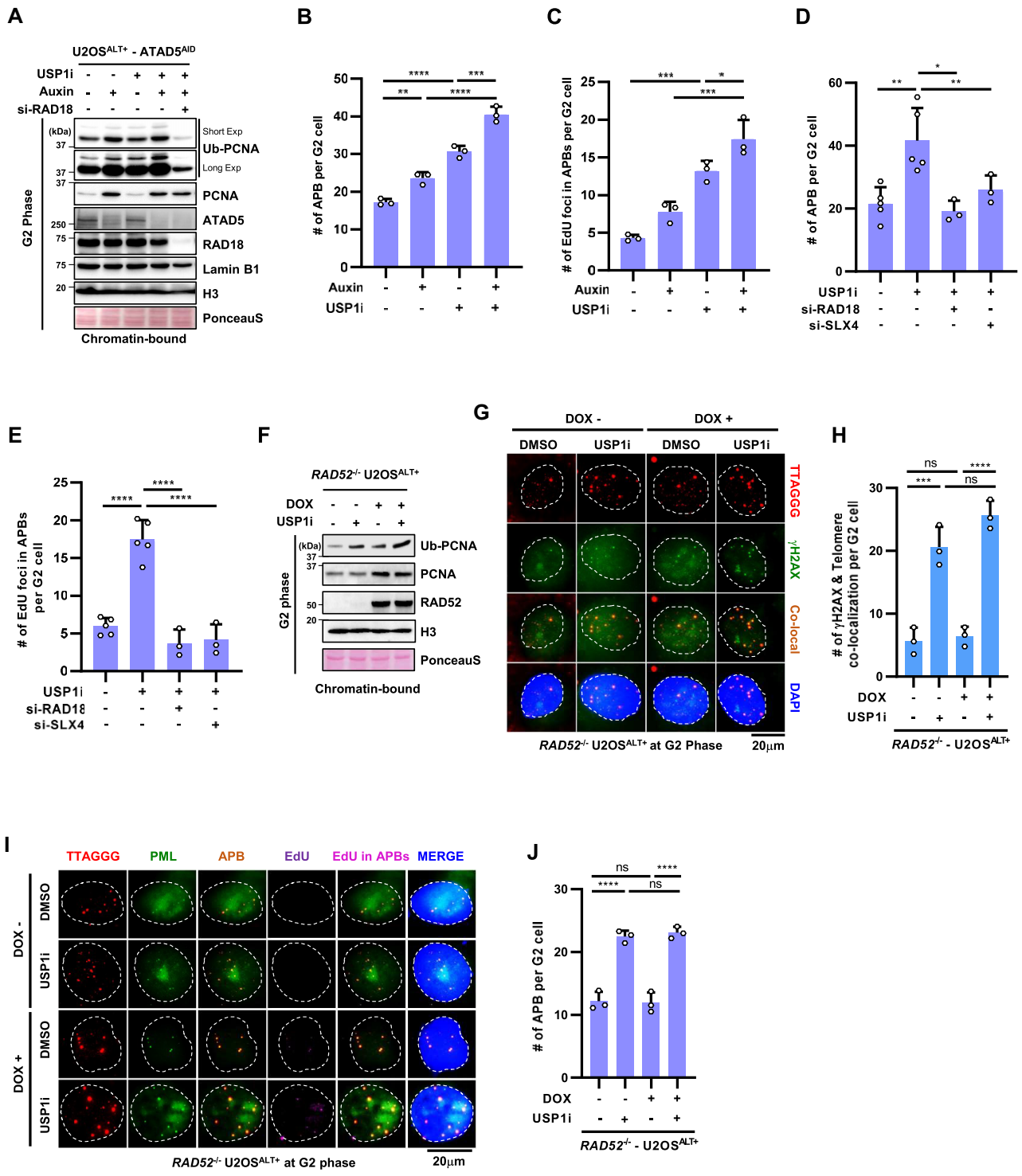

Figure 5. Ub-PCNA triggers telomere damage leading to APB formation and subsequent BIR in the G2 phase of ALT + cancer cells (**A–C**) U2OS-ATAD5^{AID} cells were synchronized in the G2 phase, treated with auxin and/or USP1i for 6 h, and chromatin-bound protein extracts were prepared for immunoblotting (A) or cells were subjected to an ATSA assay (B,C). (**D,E**) After transfection, U2OS cells were synchronized in the G2 phase, treated with USP1i for 6 h, and subjected to an ATSA assay. (**F–J**) RAD52 doxycycline-inducible *RAD52*$^{-/-}$ U2OS cells were synchronized in the G2 phase, treated with USP1i for 6 h, and chromatin-bound protein extracts were prepared for immunoblotting (**F**) or cells were fixed for gH2AX immunostaining to measure TIFs (**G,H**) or an ATSA assay (**I,J**). RAD52 expression was induced by doxycycline (DOX) treatment for 48 h before cell harvest or fixation. (**G,I**) Representative images. The dotted line represents the edge of the nucleus. Data in all graphs represent the mean ± s.d. of at least three independent experiments. Statistical analysis: One-way ANOVA (B-E, H, J). ****P<0.0001, ***P<0.001, **P<0.01, *P<0.05 and ns.: not significant.

unprocessed Ub-PCNA during the G2 phase can trigger telomere damage, leading to APB formation before subsequent BIR.

The TLS polymerase REV1 is dispensable for increased APB numbers caused by unprocessed ub-PCNA in the G2 phase

MonoUb-PCNA recruits Y-family TLS polymerases to bypass DNA lesions (28). REV1, a pivotal TLS polymerase, was reported to be required for MiDAS (45). We therefore investigated the involvement of TLS in the increased APB numbers caused by Ub-PCNA in the G2 phase. Treatment of U2OS cells in the G2 phase with a REV1 inhibitor (REV1i), JH-RE-06 (66), did not affect the number of total APBs and EdU + APBs (Supplementary Figure S5C,D). In addition, USP1i-induced APBs and EdU + APBs were not affected by REV1i, suggesting that TLS is not involved in the increased APBs induced by unprocessed Ub-PCNA.

SLX4 participates in ub-PCNA-induced APB formation

SLX4 promotes BIR-like MiDAS at CFSs and telomeres (20,58). In addition, SLX4 is reported to be recruited to DNA damage sites via its ubiquitin-binding zinc finger 4 (UBZ4) domain (48,67,68). Because unprocessed Ub-PCNA due to ATAD5 depletion or USP1i treatment induces telomere damage and APB formation, we investigated whether SLX4 is involved in the process. Interestingly, we found that SLX4 depletion restored the USP1i-induced increases in APBs and EdU + APBs to the levels similar to those achieved by RAD18 depletion in the G2 phase (Figure 5D,E and Supplementary Figure S5B), suggesting a possible role of SLX4 in the enhancement of ALT activity associated with unprocessed Ub-PCNA.

Ub-PCNA increases SLX4 recruitment to telomeres in ALT + cells, but not in TEL + cells in the G2 phase

Since SLX4 is involved in ALT regulation, we next investigated the effects of Ub-PCNA on telomeric localization of SLX4 in U2OS cells. As previously reported (69,70), a portion of SLX4 foci colocalized with telomeres in the G2 phase (Figure 6A,B). The localization of SLX4 at telomeres was increased by ATAD5 depletion but decreased by RAD18 depletion. Furthermore, the enhanced localization of SLX4 at telomeres induced by ATAD5 depletion was reduced by RAD18 co-depletion. G2-specific ATAD5 degradation or USP1i treatment also increased SLX4 localization at telomeres in U2OS-ATAD5^{AID} cells (Figure 6C). In contrast, telomeric SLX4 localization was not affected by G2-specific USP1 inhibition in HeLa_LT cells (Figure 6D and Supplementary Figure S6A). Taken together, these results suggest that unprocessed Ub-PCNA during the G2 phase facilitates SLX4 recruitment to telomeres in ALT + cells.

SLX4 is recruited to telomeres containing polyUb-PCNA in a UBZ4 domain-dependent manner

DiUb- and polyUb-PCNA was detected after G2-specific ATAD5 degradation or USP1i treatment in U2OS cells but not in HeLa_LT cells (Figure 5A and Supplementary Figures S5A and S6A). SLX4 is recruited to interstrand crosslink lesions by interacting with K63-linked polyubiquitin chains through its UBZ4 domain (48,67,68). Since UBE2N-mediated PCNA polyubiquitination is also K63-linked (71), we determined whether SLX4 recruitment to telomeres requires polyUb-PCNA by observing SLX4 recruitment to telomeres upon downregulating PCNA deubiquitination. We first combined G2-specific ATAD5 degradation with USP1i treatment using U2OS-ATAD5^{AID} cells to increase chromatin polyUb-PCNA levels. Under these conditions, treatment with a UBE2N inhibitor (UBE2Ni), NSC697923 downregulated PCNA polyubiquitination (72) (Supplementary Figure S6B) and reduced SLX4 localization at telomeres to basal levels (Figure 6E), strongly suggesting that polyUb-PCNA recruits SLX4 to telomeres in ALT + cells.

Telomeric G4 signals are frequently found in ALT + cancer cells and G4 stabilization promotes ALT activity (8,21,24). We found that a G4 stabilizer pyridostatin (PDS) treatment increased both monoUb- and diUb-PCNA levels on chromatin in two different ALT + cancer cell lines (Supplementary Figure S6C). The colocalization of SLX4 foci with telomeres was also increased by PDS treatment, which was reduced to basal levels by RAD18 depletion or UBE2Ni treatment (Figure 6F,G and Supplementary Figure S6D), suggesting sustained G4s recruit SLX4 to telomeres via PCNA polyubiquitination in ALT + cancer cells.

Next, we investigated the role of the UBZ4 domain of SLX4 in its recruitment to telomeres with unprocessed Ub-PCNA during the G2 phase. We used U2OS cells expressing the following SLX4 constructs, each fused to a green fluorescent protein (GFP) (48): full-length SLX4 (SLX4^{FL}), N-terminal fragment of SLX4 (SLX4^{N}), and SLX4^{N} with a mutation in the UBZ4-1 (SLX4$^{UBZ4\text{-}1m}$), UBZ4-2 (SLX4$^{UBZ4\text{-}2m}$), or both UBZ4 domains (SLX4$^{UBZ4\text{-}1/2m}$) (Figure 6G,H and Supplementary Figure S7A). Protein expression levels and foci numbers in the G2 phase were comparable among SLX4^{N} and the three SLX4^{N} mutants (Supplementary Figure S7B,C). USP1 inhibition increased SLX4^{FL} localization at telomeres in U2OS cells (Figure 6H,I). SLX4^{N} exhibited less localization at telomeres than SLX4^{FL}, probably due to the lack of a TBM domain. Interestingly, SLX4$^{UBZ4\text{-}1m}$, SLX4$^{UBZ4\text{-}2m}$ and SLX4$^{UBZ4\text{-}1/2m}$ showed significantly reduced localization at telomeres compared with SLX4^{N} under USP1i-treated conditions (Figure 6H and I). Taken together, these data suggest that SLX4 is recruited to polyUb-PCNA at telomeres through its UBZ4 domain.

Unprocessed polyUb-PCNA induces APB formation and MiDAS at telomeres and CFS

Consistent with the role of polyUb-PCNA in SLX4 recruitment to telomeres, UBE2N inhibition restored the increases in APBs including EdU + APBs induced by G2-specific ATAD5 degradation and USP1i treatment in U2OS-ATAD5^{AID} cells (Figure 7A,B). These results strongly suggest that the recruitment of SLX4 to telomeres by polyUb-PCNA is responsible for telomere damage and subsequent APB formation in ALT + cells.

BIR-like MiDAS at telomeres and CFS requires SLX4 (20,58). Inspired by the findings that polyUb-PCNA is involved in the recruitment of SLX4 for BIR initiation at telomeres, we investigated the involvement of polyUb-PCNA in MiDAS. UBE2N inhibition alone reduced MiDAS at both telomeres and CFSs in U2OS cells (Figure 7C–E). Consistently, UBE2N inhibition reversed the increased MiDAS by USP1 depletion (Figure 7C–E). Furthermore, UBE2N inhibition

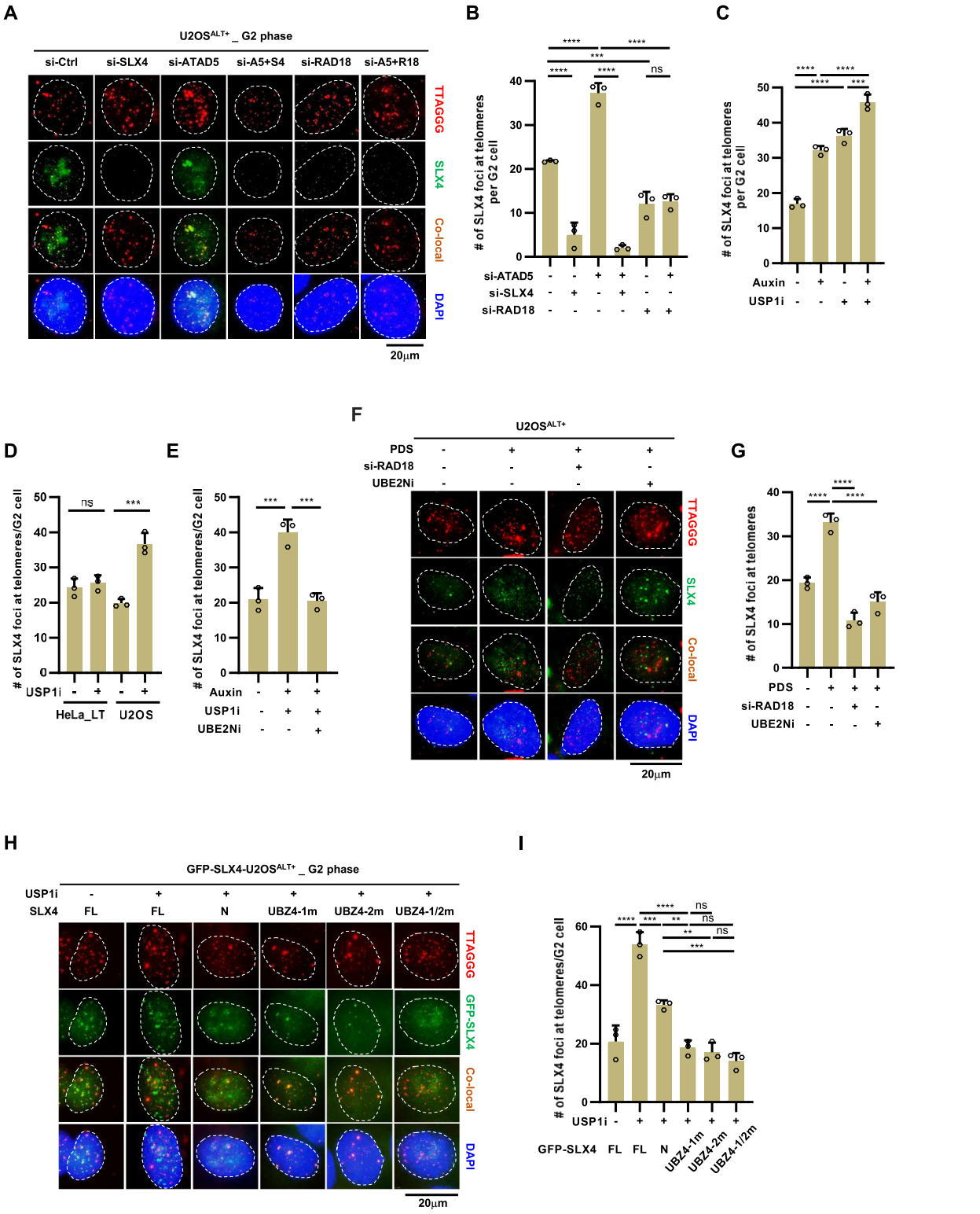

Figure 6. PolyUb-PCNA increases SLX4 recruitment to telomeres in ALT + cancer cells. (**A,B**) After transfection, U2OS cells were synchronized in G2 phase and fixed for SLX4 immunostaining with telomere FISH. (A) Representative images showing SLX4 localization at telomeres. The dotted line represents the edge of the nucleus. (B–F,H) The number of SLX4 localization at telomeres in the G2 phase was quantified. (**C**) U2OS-ATAD5^{AID} synchronized in the G2 phase were treated with auxin and USP1i for 6 h and fixed. (**D**) HeLa_LT or U2OS cells synchronized in the G2 phase were treated with USP1i for 6 h and fixed. (**E**) G2-synchronized U2OS-ATAD5^{AID} cells were treated with auxin, USP1i, and UBE2Ni for 6 h, and cells were fixed. (**F,G**) After siRNA transfection, U2OS cells were treated with PDS for 24 h and UBE2Ni for 6 h, respectively, before fixation. (F) Representative images. (**H,I**) U2OS cells expressing GFP-tagged full-length SLX4 (FL), N-terminal fragment of SLX4 (**N**), SLX4^{N} with a mutation in UBZ4-1 (UBZ4-1m), UBZ4-2 (UBZ4-2m) or both UBZ4 domains (UBZ4-1/2m), respectively, were synchronized in the G2 phase, treated with USP1i for 6 h and fixed. (H) Representative images showing GFP-SLX4 localization at telomeres. The dotted line represents the edge of the nucleus. Data in all graphs represent the mean ± s.d. of at least three independent experiments. Statistical analysis: One-way ANOVA (B,C,E,G,I); two-tailed unpaired Student's *t*-test (D). ****P<0.0001, ***P<0.001, **P<0.01, *P<0.05 and ns.: not significant.

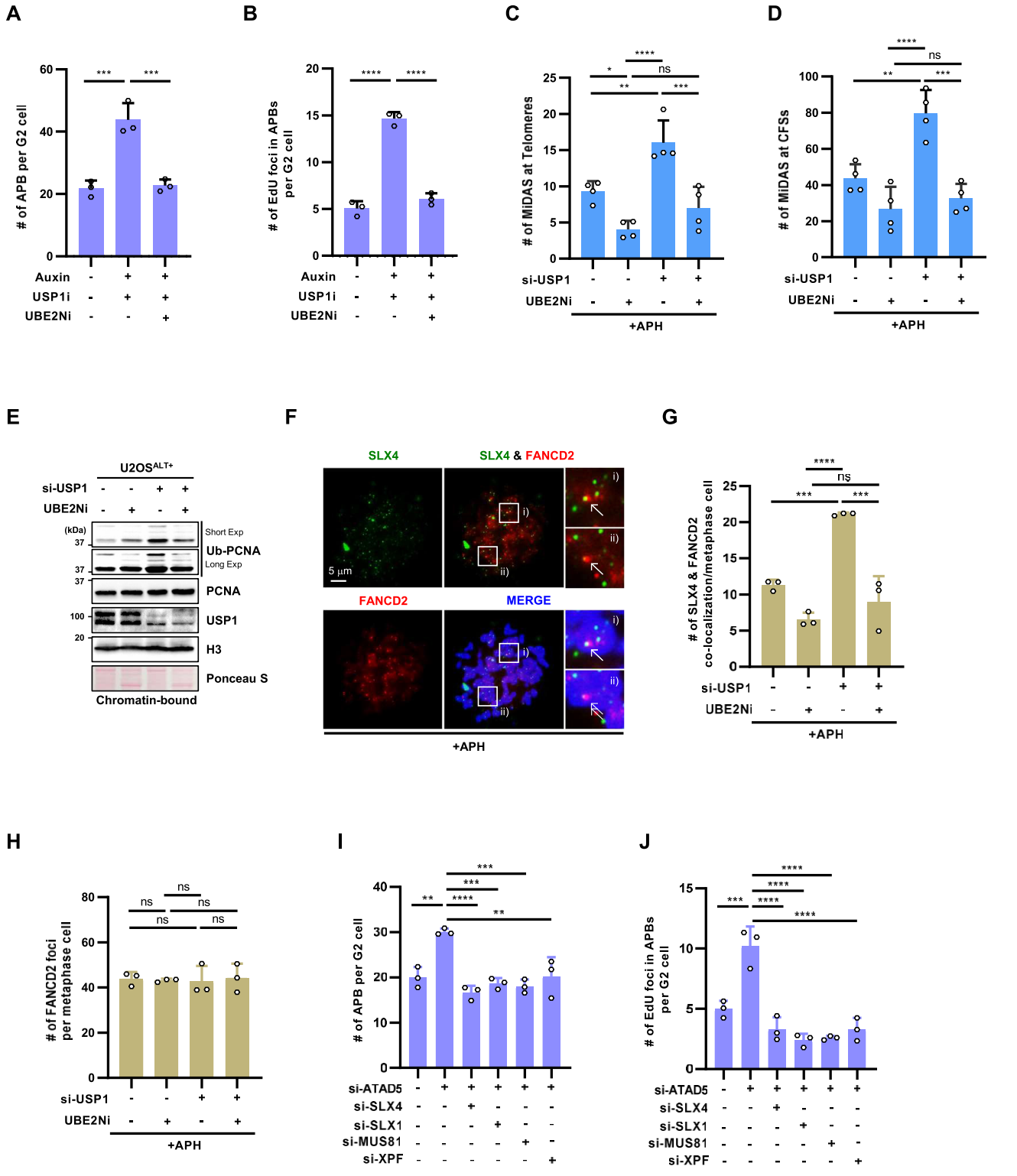

Figure 7. PolyUb-PCNA induces APB formation and MiDAS at telomeres and CFS. (**A,B**) G2-synchronized (G2) U2OS-ATAD5^{AID} cells were treated with auxin, USP1i and UBE2Ni for 6 h, and cells were fixed for an ATSA assay. (**C–H**) After transfection, U2OS cells were subjected to a MiDAS assay (C,D), immunoblotting with chromatin-bound protein extracts (E), or immunostaining (F–H). (C,D,F–H) U2OS cells were treated with 0.4 mM aphidicolin (APH) for 16 h, and 10 mM UBE2Ni for 17 h before fixation as indicated. (C,D) The number of MiDAS at telomeres (C) or CFSs (D) was quantified. (F) Representative images showing SLX4 and FANCD2 localization in metaphase cells. (G,H) The number of SLX4 and FANCD2 co-localization (G) and FANCD2 foci (H) per metaphase cell was quantified. (I,J) After transfection, U2OS cells synchronized in the G2 phase were fixed for an ATSA assay. Data in all graphs represent the mean ± s.d. of at least three independent experiments. Statistical analysis: One-way ANOVA (A–D, G–J). ****P<0.0001, ***P<0.001, **P<0.01, *P<0.05 and ns.: not significant.

reduced SLX4 localization at FANCD2 foci, which are associated with CFS expression in metaphase (73), and restored the increases induced by USP1 depletion in U2OS cells (Figure 7F,G), while the number of FANCD2 foci remained constant (Figure 7H). Taken together, these results suggest that polyUb-PCNA-mediated SLX4 recruitment is responsible for BIR-like MiDAS at telomeres and CFS in ALT + cells.

SLX4-interacting nucleases facilitate APB formation and telomeric DNA synthesis in ATAD5-deficient ALT + cells

SLX4 is a scaffold for several nucleases such as SLX1, MUS81-EME1, and XPF-ERCC1 (74). We investigated which of these nucleases is responsible for the increased ALT activity associated with unprocessed Ub-PCNA in ALT + cells. Unexpectedly, depletion of any of the three nucleases restored the increases in total APBs and EdU + APBs induced by ATAD5 depletion to levels similar to those caused by SLX4 co-depletion (Figure 7I,J and Supplementary Figure S7D,E). These results suggest that SLX1, MUS81-EME1, and XPF-ERCC1 cooperatively generate DNA breaks at telomeres associated with polyUb-PCNA, leading to APB formation and ALT processes.

Discussion

PCNA ubiquitination plays a crucial role in directing damage bypass pathway and occurs during DNA replication and DNA repair synthesis (29–31,75). Our study reveals the role of Ub-PCNA in BIR-associated ALT processes during the G2 phase. We propose that polyUb-PCNA contributes to these processes by inducing telomere breakage and facilitating RAD52-dependent BIR [Figure 8A (i)–(iii)]. We found that polyUb-PCNA at telomeres recruits SLX4 and SLX4-interacting nucleases, leading to telomere breaks and APB formation. Inhibition of PCNA polyubiquitination reduced APB levels and telomeric MiDAS events in ALT + cells. Suppression of USP1-mediated PCNA deubiquitination during the G2 phase increased TIF signals and APB levels specifically in ALT + cells in a RAD18-, UBE2N- and SLX4-dependent manner. Consistently, ATAD5 or USP1 deficiency increased telomeric BIR-like MiDAS events in a RAD18-, UBE2N- and RAD52-dependent manner. In addition, unprocessed Ub-PCNA during the G2 phase increased telomeric SLX4 localization, dependent on RAD18, UBE2N and SLX4 UBZ4 domain. It is unclear whether polyUb-PCNA-SLX4-mediated telomere breakage also occurs during the S phase. However, because APBs have been reported to be enriched in the G2 phase in ALT + cells (57), the event is more likely to occur in the G2 phase. Excessive telomeric DNA breakage and recombination caused by uncontrolled polyUb-PCNA-SLX4 activity can lead to telomere instability [Figure 8B (i)]. Therefore, this activity must be limited to tolerable levels, and this counterbalance likely relies on proper deubiquitination and/or unloading of polyUb-PCNA by the USP1-UAF1-ATAD5-RLC [Figure 8A (ii)]. Additionally, we propose that Ub-PCNA enhances the BIR process in ALT + cells [Figure 8A (iv)], as observed through its localization at telomeric break sites and the promotion of break-induced telomere DNA synthesis. Overall, Ub-PCNA serves as both an inducer of telomere breakage and a promoter of the BIR process in BIR-associated ALT processes.

We observed RAD18- and UBE2N-dependent MiDAS events not only at telomeres but also at CFSs in ALT + U2OS cells. UBE2N inhibition decreased SLX4 localization at FANCD2 foci (sites of CFS expression) in metaphase, while USP1 depletion increased it in a UBE2N-dependent manner, similar to telomeres. We speculate that the molecular mechanisms associated with polyUb-PCNA are primarily utilized to alleviate replication stress of telomeres, potentially leading to an increase in replication stress at CFSs in ALT + cells. In addition, CFS, which has longer replication times and is sensitive to replication stress (76), may be particularly dependent on the polyUb-PCNA-associated BIR mechanism. Interestingly, a high-resolution mapping study in U2OS cells showed that there are additional MiDAS regions that do not overlap with HeLa cells (77), possibly corresponding to CFSs regulated by polyUb-PCNA-associated BIR mechanisms in U2OS cells.

Our study found that ALT + cancer cells exhibited increased MiDAS events and recombination-associated ALT phenotypes due to unprocessed Ub-PCNA, while TEL + HeLa_LT cells did not. The ALT cell-specific effect may be attributed to the higher levels of replication stress inherent in ALT telomeres (78). We observed higher monoUb-PCNA levels in ALT + U2OS cells compared to TEL + HeLa_LT cells, and polyUb-PCNA was only present in U2OS cells, particularly after G2-specific USP1 inhibition (Supplementary Figure S5A and S6A). These differences in polyUb-PCNA levels may lead to SLX4-mediated telomeric breakage specifically in ALT + cells. The lower levels of Ub-PCNA in HeLa_LT cells despite increased levels of RAD18 protein seem puzzling (Supplementary Figure S6A). We believe that high RAD18 protein levels are not significantly associated with PCNA ubiquitination in HeLa cells. According to Garcia-Exposito *et al.* (56), RAD18 is enriched with telomeric DNA only in U2OS cells but not in HeLa cells. This suggests that replication stress itself, which induces replication fork stalling and single-strand DNA exposure, is more critical for RAD18 recruitment and subsequent PCNA ubiquitination. The presence of APBs, which contain various recombination and replication proteins (7,8,13), in ALT + cells may provide opportunities for RAD52-mediated BIR that can be triggered by ATAD5 deficiency or USP1 inhibition. In addition, ALT telomeres, which are characterized by greater replication difficulties, may require more Ub-PCNA for the BIR process compared to TEL telomeres. For these reasons, we suggest that the effects of Ub-PCNA in promoting telomeric BIR and ALT phenotypes may be specific to ALT + cells.

The concept of 'MiDAS' has been challenged following a recent paper which demonstrated the off-target activity of RO3306 leading to impairment of G2 DNA replication under normal and mild replication stress conditions (18). Accordingly, the paper considered the 'MiDAS assay using RO3306' as an indicator of the resumption of DNA synthesis in mitosis. However, there is still an argument that at least some of the MiDAS is involved in DNA damage repair. G2 DNA replication for the late replication process and BIR-like MiDAS may be sequential processes, with the latter being increased by RO3306 treatment. This is consistent with a paper, which shows that RAD51 promotes MiDAS at both DNA damage-associated and non-DNA damage-associated loci under RO3306-treated conditions (79). The reduction of telomeric MiDAS by POLD3 depletion (Figure 2F) also supports the view that the assay represents the DNA damage repair process. Even separating two processes, G2 DNA replication and

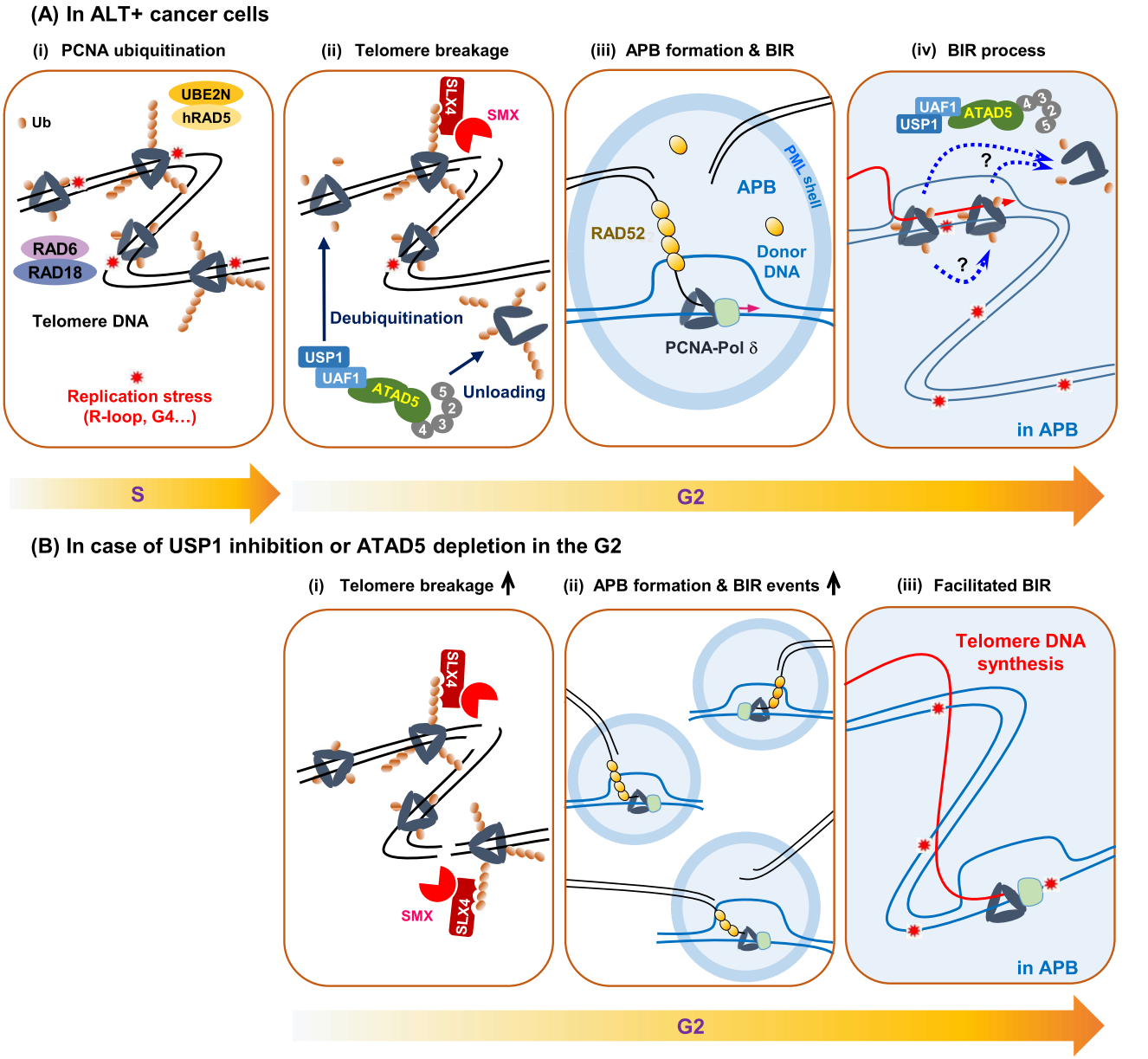

Figure 8. Graphical model of polyUb-PCNA-induced generation of telomere breakage and Ub-PCNA-induced promotion of the BIR processes in ALT + cancer cells. [**A**, (i,ii)] Telomeres in ALT + cells suffer more frequent replication stress than those in TEL + cells. MonoUb- and polyUb-PCNA, formed under telomeric replication stress, remain on chromatin at a significant level until the G2 phase due to an unknown mechanism that restricts unloading and deubiquitination of Ub-PCNA. Although it is not clear whether monoUb- and polyUb-PCNA in the G2 phase have completed their roles in TLS- and template switch-mediated damage bypass, respectively, the K63-linked-polyubiquitin chain of PCNA additionally acts as a binding site for SLX4 via the UBZ4 domain and consequently acts as a working platform for the SLX4-associated SMX tri-nuclease complex. All three endonucleases comprising the SMX tri-nuclease complex (SLX1, MUS81, and XPF) cooperatively generate telomere breakage. [A, (iii)] Broken telomeric DNA ends induce APB formation with a help of BLM helicase and PML, and then RAD52- and POLD3-dependent BIR is initiated in APBs. [A, (ii)] Telomeric breakage by polyUb-PCNA-SLX4 is inhibited by balanced deubiquitination and/or unloading of polyUb-PCNA by the USP1-UAF1-ATAD5-RLC. [**B**, (i,ii)] When this counterbalance is disrupted by acute ATAD5 depletion or USP1 inhibition, even in the G2 phase, the excess polyUb-PCNA increases the abundance of the SLX4 and SMX tri-nuclease complex at telomeres, which leads to sequential increases in telomeric breakage, APB formation, ALT phenotypes, and telomere length. [A, (iv)] During the BIR process, PCNA-polymerase δ encounters replication stress, and, consequently, PCNA is ubiquitinated. Although whether monoUb-PCNA or polyUb-PCNA is present and the role of Ub-PCNA during BIR is unclear, our results suggest that Ub-PCNA facilitates the BIR process. [B, (iii)] Consistently, Ub-PCNA left unprocessed due to depletion of ATAD5 or USP1 increased TRF1-FokI-induced telomeric DNA synthesis and telomeric MiDAS.

BIR-like MiDAS, may be unavoidable, considering a report showing replisome disassembly and fork breakage by mitotic CDK (80). Given the diverse causes of replication perturbations across the human genome, we believe it is reasonable to conclude that MiDAS arises from multiple pathways at different loci.

The PCNA-unloading-defective ATAD5^{E1173K} exhibited increased break- and recombination-associated ALT phenotypes similar to ATAD5 depletion (Figure 4), which indicates that the PCNA unloading activity of ATAD5 is necessary to limit ALT phenotypes. ATAD5^{E1173K} can facilitate PCNA deubiquitination, but it is unclear whether the PCNA promoting ALT phenotypes in cells expressing ATAD5^{E1173K} are unmodified or ubiquitinated. Ub-PCNA remains on chromatin even in the G2 phase (Supplementary Figure S5A), and monoUb-PCNA-dependent TLS levels are higher in the G2 phase compared to the S phase (81). This suggests that there is a mechanism to restrict the deubiquitination and unloading of Ub-PCNA before completing its task in the G2 phase. Therefore, we speculate that Ub-PCNA, rather than unmodified PCNA, present at telomeres in the G2 phase contributes to the augmented ALT phenotypes in cells expressing ATAD5^{E1173K}.

SLX4 localizes at telomeres by interacting with TRF2 through its TBM domain, preventing telomere damage and negatively regulating telomere length in TEL + and ALT + cancer cells (69,70). SLX4 also counteracts BLM- and POLD3-mediated telomere synthesis and ALT activity through its TBM domain in ALT + cancer cells (61). However, in the present study, a positive role of SLX4 in BIR-associated ALT processes was observed, which depended on its UBZ4 domain rather than the TBM domain. The recruitment of SLX4 to interstrand crosslink lesions occurs through its UBZ4 domain, which interacts with K63-linked polyubiquitin chains on proteins around the lesions (48,67,68). We propose that K63-linked polyUb-PCNA at telomeres serves as a binding platform for SLX4 and its associated SMX tri-nuclease complex (SLX1, MUS81-EME1 and XPF-ERCC1), leading to telomere breakage in the G2 phase. Although each structure-specific endonucleases (SLX1, MUS81 and XPF) in the SMX complex has different substrate preferences (82), all three nucleases are required for telomere breakage caused by polyUb-PCNA-SLX4 (Figure 7I,J). This requirement for all three nucleases was also observed in T-SCE in U2OS cells (69). The specific telomeric DNA structures associated with polyUb-PCNA are currently unclear, but it appears that they must be processed sequentially or cooperatively by the entire SMX tri-nuclease complex.

PCNA K164 is the binding site for small ubiquitin-like modifier (SUMO) and ubiquitin in budding yeast (29). SUMOylated PCNA (SUMO-PCNA) at K164 is also found in human cells when SUMO is overexpressed (83,84). In yeast, SUMOylated PCNA (SUMO-PCNA) at K164 or K127 is required for recruitment of the Srs2 helicase to inhibit recombination at the replication forks (85). SUMO-PCNA accumulates on chromatin in the absence of Elg1 (34), particularly during S phase, contributing to telomere elongation upon Elg1 loss (43,86). In the same report, RAD18 was not associated with telomere length, regardless of the presence of Elg1 (86). Yeast Cdc13 is known to recruit TEL to telomeres via its interaction with Est1 subunit of TEL, promoting TEL activity, and the subsequent formation of the Cdc13-Stn1-Ten (CST) complex terminates TEL activity (87–89). The beneficial effects of SUMO-PCNA on telomere elongation have been reported to be mediated by interaction with Cdc13 and subsequent enhanced TEL activity (86). Thus, in yeast, SUMO rather than ubiquitin attached to PCNA K164 is responsible for telomere elongation in the absence of Elg1. In human cells, this regulation based on SUMO-PCNA and Cdc13 interaction is not present in ALT + cells where TEL activity is lost. Furthermore, it may not be present in TEL + cells because human CTC1, a functional counterpart of yeast Cdc13 in the CTC1-STN1-TEN1 (CST) complex, is known to directly inhibit TEL recruitment to telomeres (90). SUMOylation of endogenous wild-type PCNA has not been reported in mammalian cells. Of course, this does not mean that SUMO-PCNA is not present in cells at all. In fact, an anti-recombinogenic role of overexpressed SUMO-PCNA has been reported in human cells (83,91), similar to that in yeast. Therefore, it is still worthwhile to investigate the biology of PCNA SUMOylation in mammalian cells, including the demonstration of its presence.

Data availability

All data are available in the main text or the supplementary materials.

Supplementary data

Supplementary Data are available at NAR Online.

Acknowledgements

We thank Dr. Roger A. Greenberg, Dr. Lee Zou, Dr. Jan Karlseder, and Dr. Minoru Takata for generously providing and sharing technical information about the U2OS-mCherry-TRF1-FokI cells, the RAD52 inducible U2OS-*RAD52*$^{-/-}$ (clone #2) cells, the HeLa_LT cells, and the CSII-based SLX4 DNA constructs, respectively. We also thank RIKEN BRC for the MTA agreement (#DNA86581) on the CSII-based SLX4 DNA constructs. We sincerely thank members of the Center for Genomic Integrity, IBS for helpful discussions and comments. S.K. is thankful for the support of the ASAN Foundation Biomedical Science scholarship.

Funding

Institute for Basic Science [IBS-R022-D1]; National Research Foundation of Korea (NRF) grant funded by the Korea government (MSIT) [RS-2023-00251939]; National Research Foundation of Korea (NRF) grant funded by the Korea government (MSIT) [RS-2024-00349478]. Funding for open access charge: Institute for Basic Science [IBS-R022-D1].

Conflict of interest statement

No potential conflict of interest was reported by the author(s).

References

1. Shay,J.W. (2016) Role of Telomeres and telomerase in aging and cancer. *Cancer Discov.*, **6**, 584–593.
2. De Vitis,M., Berardinelli,F. and Sgura,A. (2018) Telomere length maintenance in cancer: at the crossroad between Telomerase and alternative lengthening of Telomeres (ALT). *Int. J. Mol. Sci.*, **19**, 606.

3. Kim,N.W., Piatyszek,M.A., Prowse,K.R., Harley,C.B., West,M.D., Ho,P.L., Coviello,G.M., Wright,W.E., Weinrich,S.L. and Shay,J.W. (1994) Specific association of human telomerase activity with immortal cells and cancer. *Science*, **266**, 2011–2015.
4. Bryan,T.M., Englezou,A., Dalla-Pozza,L., Dunham,M.A. and Reddel,R.R. (1997) Evidence for an alternative mechanism for maintaining telomere length in human tumors and tumor-derived cell lines. *Nat. Med.*, **3**, 1271–1274.
5. Cesare,A.J. and Reddel,R.R. (2010) Alternative lengthening of telomeres: models, mechanisms and implications. *Nat. Rev. Genet.*, **11**, 319–330.
6. Roumelioti,F.M., Sotiriou,S.K., Katsini,V., Chiourea,M., Halazonetis,T.D. and Gagos,S. (2016) Alternative lengthening of human telomeres is a conservative DNA replication process with features of break-induced replication. *EMBO Rep.*, **17**, 1731–1737.
7. Zhang,J.M., Yadav,T., Ouyang,J., Lan,L. and Zou,L. (2019) Alternative lengthening of Telomeres through two distinct break-induced replication pathways. *Cell Rep.*, **26**, 955–968.
8. Min,J., Wright,W.E. and Shay,J.W. (2017) Alternative lengthening of telomeres mediated by mitotic DNA synthesis engages break-induced replication processes. *Mol. Cell. Biol.*, **37**, e00226-17.
9. Zhang,J.M. and Zou,L. (2020) Alternative lengthening of telomeres: from molecular mechanisms to therapeutic outlooks. *Cell Biosci.*, **10**, 30.
10. Malkova,A. and Ira,G. (2013) Break-induced replication: functions and molecular mechanism. *Curr. Opin. Genet. Dev.*, **23**, 271–279.
11. Costantino,L., Sotiriou,S.K., Rantala,J.K., Magin,S., Mladenov,E., Helleday,T., Haber,J.E., Iliakis,G., Kallioniemi,O.P. and Halazonetis,T.D. (2014) Break-induced replication repair of damaged forks induces genomic duplications in human cells. *Science*, **343**, 88–91.
12. Anand,R.P., Lovett,S.T. and Haber,J.E. (2013) Break-induced DNA replication. *Cold Spring Harb. Perspect. Biol.*, **5**, a010397.
13. Draskovic,I., Arnoult,N., Steiner,V., Bacchetti,S., Lomonte,P. and Londono-Vallejo,A. (2009) Probing PML body function in ALT cells reveals spatiotemporal requirements for telomere recombination. *Proc. Natl. Acad. Sci. USA*, **106**, 15726–15731.
14. Yeager,T.R., Neumann,A.A., Englezou,A., Huschtscha,L.I., Noble,J.R. and Reddel,R.R. (1999) Telomerase-negative immortalized human cells contain a novel type of promyelocytic leukemia (PML) body. *Cancer Res.*, **59**, 4175–4179.
15. Bhowmick,R. and Hickson,I.D. (2017) The "enemies within": regions of the genome that are inherently difficult to replicate. *F1000Res*, **6**, 666.
16. Petermann,E., Lan,L. and Zou,L. (2022) Sources, resolution and physiological relevance of R-loops and RNA-DNA hybrids. *Nat. Rev. Mol. Cell Biol.*, **23**, 521–540.
17. Maffia,A., Ranise,C. and Sabbioneda,S. (2020) From R-loops to G-quadruplexes: emerging new threats for the replication fork. *Int. J. Mol. Sci.*, **21**, 1506.
18. Mocanu,C., Karanika,E., Fernandez-Casanas,M., Herbert,A., Olukoga,T., Ozgurses,M.E. and Chan,K.L. (2022) DNA replication is highly resilient and persistent under the challenge of mild replication stress. *Cell Rep.*, **39**, 110701.
19. Bhowmick,R., Minocherhomji,S. and Hickson,I.D. (2016) RAD52 Facilitates mitotic DNA synthesis following replication stress. *Mol. Cell*, **64**, 1117–1126.
20. Ozer,O., Bhowmick,R., Liu,Y. and Hickson,I.D. (2018) Human cancer cells utilize mitotic DNA synthesis to resist replication stress at telomeres regardless of their telomere maintenance mechanism. *Oncotarget*, **9**, 15836–15846.
21. Yang,S.Y., Chang,E.Y.C., Lim,J., Kwan,H.H., Monchaud,D., Yip,S., Stirling,P.C. and Wong,J.M.Y. (2021) G-quadruplexes mark alternative lengthening of telomeres. *NAR Cancer*, **3**, zcab031.
22. Silva,B., Pentz,R., Figueira,A.M., Arora,R., Lee,Y.W., Hodson,C., Wischnewski,H., Deans,A.J. and Azzalin,C.M. (2019) FANCM limits ALT activity by restricting telomeric replication stress induced by deregulated BLM and R-loops. *Nat. Commun.*, **10**, 2253.
23. Pan,X., Drosopoulos,W.C., Sethi,L., Madireddy,A., Schildkraut,C.L. and Zhang,D. (2017) FANCM, BRCA1, and BLM cooperatively resolve the replication stress at the ALT telomeres. *Proc. Natl. Acad. Sci. USA*, **114**, E5940–E5949.
24. Amato,R., Valenzuela,M., Berardinelli,F., Salvati,E., Maresca,C., Leone,S., Antoccia,A. and Sgura,A. (2020) G-quadruplex stabilization fuels the ALT pathway in ALT-positive osteosarcoma cells. *Genes (Basel)*, **11**, 304.
25. Arora,R., Lee,Y., Wischnewski,H., Brun,C.M., Schwarz,T. and Azzalin,C.M. (2014) RNaseH1 regulates TERRA-telomeric DNA hybrids and telomere maintenance in ALT tumour cells. *Nat. Commun.*, **5**, 5220.
26. Pan,X., Chen,Y., Biju,B., Ahmed,N., Kong,J., Goldenberg,M., Huang,J., Mohan,N., Klosek,S., Parsa,K., *et al.* (2019) FANCM suppresses DNA replication stress at ALT telomeres by disrupting TERRA R-loops. *Sci. Rep.*, **9**, 19110.
27. Vohhodina,J., Goehring,L.J., Liu,B., Kong,Q., Botchkarev,V.V., Huynh,M., Liu,Z., Abderazzaq,F.O., Clark,A.P., Ficarro,S.B, *et al.*2021) BRCA1 binds TERRA RNA and suppresses R-loop-based telomeric DNA damage. *Nat. Commun.*, **12**, 3542.
28. Moldovan,G.L., Pfander,B. and Jentsch,S. (2007) PCNA, the maestro of the replication fork. *Cell*, **129**, 665–679.
29. Hoege,C., Pfander,B., Moldovan,G.L., Pyrowolakis,G. and Jentsch,S. (2002) RAD6-dependent DNA repair is linked to modification of PCNA by ubiquitin and SUMO. *Nature*, **419**, 135–141.
30. Motegi,A., Liaw,H.J., Lee,K.Y., Roest,H.P., Maas,A., Wu,X., Moinova,H., Markowitz,S.D., Ding,H., Hoeijmakers,J.H., *et al.* (2008) Polyubiquitination of proliferating cell nuclear antigen by HLTF and SHPRH prevents genomic instability from stalled replication forks. *Proc. Natl. Acad. Sci. USA*, **105**, 12411–12416.
31. Unk,I., Hajdu,I., Fatyol,K., Hurwitz,J., Yoon,J.H., Prakash,L., Prakash,S. and Haracska,L. (2008) Human HLTF functions as a ubiquitin ligase for proliferating cell nuclear antigen polyubiquitination. *Proc. Natl. Acad. Sci. USA*, **105**, 3768–3773.
32. Kang,M.S., Ryu,E., Lee,S.W., Park,J., Ha,N.Y., Ra,J.S., Kim,Y.J., Kim,J., Abdel-Rahman,M., Park,S.H., *et al.* (2019) Regulation of PCNA cycling on replicating DNA by RFC and RFC-like complexes. *Nat. Commun.*, **10**, 2420.
33. Lee,K.Y., Fu,H., Aladjem,M.I. and Myung,K. (2013) ATAD5 regulates the lifespan of DNA replication factories by modulating PCNA level on the chromatin. *J. Cell Biol.*, **200**, 31–44.
34. Kubota,T., Nishimura,K., Kanemaki,M.T. and Donaldson,A.D. (2013) The Elg1 replication factor C-like complex functions in PCNA unloading during DNA replication. *Mol. Cell*, **50**, 273–280.
35. Lee,K.Y., Yang,K., Cohn,M.A., Sikdar,N., D'Andrea,A.D. and Myung,K. (2010) Human ELG1 regulates the level of ubiquitinated proliferating cell nuclear antigen (PCNA) through its interactions with PCNA and USP1. *J. Biol. Chem.*, **285**, 10362–10369.
36. Kim,S., Kang,N., Park,S.H., Wells,J., Hwang,T., Ryu,E., Kim,B.G., Hwang,S., Kim,S.J., Kang,S., *et al.* (2020) ATAD5 restricts R-loop formation through PCNA unloading and RNA helicase maintenance at the replication fork. *Nucleic Acids Res.*, **48**, 7218–7238.
37. Park,S.H., Kang,N., Song,E., Wie,M., Lee,E.A., Hwang,S., Lee,D., Ra,J.S., Park,I.B., Park,J., *et al.* (2019) ATAD5 promotes replication restart by regulating RAD51 and PCNA in response to replication stress. *Nat. Commun.*, **10**, 5718.
38. Park,S.H., Kim,Y., Ra,J.S., Wie,M.W., Kang,M.S., Kang,S., Myung,K. and Lee,K.Y. (2021) Timely termination of repair DNA synthesis by ATAD5 is important in oxidative DNA damage-induced single-strand break repair. *Nucleic Acids Res.*, **49**, 11746–11764.
39. Lee,K.Y. and Park,S.H. (2020) Eukaryotic clamp loaders and unloaders in the maintenance of genome stability. *Exp. Mol. Med.*, **52**, 1948–1958.

40. Gali,V.K., Dickerson,D., Katou,Y., Fujiki,K., Shirahige,K., Owen-Hughes,T., Kubota,T. and Donaldson,A.D. (2018) Identification of Elg1 interaction partners and effects on post-replication chromatin re-formation. *PLoS Genet*., **14**, e1007783.
41. Smolikov,S., Mazor,Y. and Krauskopf,A. (2004) ELG1, a regulator of genome stability, has a role in telomere length regulation and in silencing. *Proc. Natl. Acad. Sci. USA*, **101**, 1656–1661.
42. Banerjee,S. and Myung,K. (2004) Increased genome instability and telomere length in the elg1-deficient Saccharomyces cerevisiae mutant are regulated by S-phase checkpoints. *Euk. Cell*, **3**, 1557–1566.
43. Johnson,C., Gali,V.K., Takahashi,T.S. and Kubota,T. (2016) PCNA retention on DNA into G2/M phase causes genome instability in cells lacking Elg1. *Cell Rep*., **16**, 684–695.
44. Lydeard,J.R., Lipkin-Moore,Z., Sheu,Y.J., Stillman,B., Burgers,P.M. and Haber,J.E. (2010) Break-induced replication requires all essential DNA replication factors except those specific for pre-RC assembly. *Genes Dev*., **24**, 1133–1144.
45. Wu,W., Barwacz,S.A., Bhowmick,R., Lundgaard,K., Goncalves Dinis,M.M., Clausen,M., Kanemaki,M.T. and Liu,Y. (2023) Mitotic DNA synthesis in response to replication stress requires the sequential action of DNA polymerases zeta and delta in human cells. *Nat. Commun*., **14**, 706.
46. Zhang,T., Rawal,Y., Jiang,H., Kwon,Y., Sung,P. and Greenberg,R.A. (2023) Break-induced replication orchestrates resection-dependent template switching. *Nature*, **619**, 201–208.
47. Dilley,R.L., Verma,P., Cho,N.W., Winters,H.D., Wondisford,A.R. and Greenberg,R.A. (2016) Break-induced telomere synthesis underlies alternative telomere maintenance. *Nature*, **539**, 54–58.
48. Katsuki,Y., Abe,M., Park,S.Y., Wu,W., Yabe,H., Yabe,M., van Attikum,H., Nakada,S., Ohta,T., Seidman,M.M., *et al.* (2021) RNF168 E3 ligase participates in ubiquitin signaling and recruitment of SLX4 during DNA crosslink repair. *Cell Rep*., **37**, 109879.
49. Baerlocher,G.M., Vulto,I., de Jong,G. and Lansdorp,P.M. (2006) Flow cytometry and FISH to measure the average length of telomeres (flow FISH). *Nat. Protoc*., **1**, 2365–2376.
50. Kimura,M., Stone,R.C., Hunt,S.C., Skurnick,J., Lu,X., Cao,X., Harley,C.B. and Aviv,A. (2010) Measurement of telomere length by the southern blot analysis of terminal restriction fragment lengths. *Nat. Protoc*., **5**, 1596–1607.
51. Margalef,P., Kotsantis,P., Borel,V., Bellelli,R., Panier,S. and Boulton,S.J. (2018) Stabilization of reversed replication forks by Telomerase drives Telomere catastrophe. *Cell*, **172**, 439–453.
52. Williams,E.S. and Bailey,S.M. (2009) Chromosome orientation fluorescence in situ hybridization (CO-FISH). *Cold Spring Harb. Protoc*., **2009**, pdb prot5269.
53. Henson,J.D., Cao,Y., Huschtscha,L.I., Chang,A.C., Au,A.Y., Pickett,H.A. and Reddel,R.R. (2009) DNA C-circles are specific and quantifiable markers of alternative-lengthening-of-telomeres activity. *Nat. Biotechnol*., **27**, 1181–1185.
54. Wu,W., Bhowmick,R., Vogel,I., Ozer,O., Ghisays,F., Thakur,R.S., Sanchez de Leon,E., Richter,P.H., Ren,L., Petrini,J.H., *et al.* (2020) RTEL1 suppresses G-quadruplex-associated R-loops at difficult-to-replicate loci in the human genome. *Nat. Struct. Mol. Biol*., **27**, 424–437.
55. Zhang,J.M., Genois,M.M., Ouyang,J., Lan,L. and Zou,L. (2021) Alternative lengthening of telomeres is a self-perpetuating process in ALT-associated PML bodies. *Mol. Cell*, **81**, 1027–1042.
56. Garcia-Exposito,L., Bournique,E., Bergoglio,V., Bose,A., Barroso-Gonzalez,J., Zhang,S., Roncaioli,J.L., Lee,M., Wallace,C.T., Watkins,S.C., *et al.* (2016) Proteomic profiling reveals a specific role for translesion DNA polymerase eta in the alternative lengthening of telomeres. *Cell Rep*., **17**, 1858–1871.
57. Grobelny,J.V., Godwin,A.K. and Broccoli,D. (2000) ALT-associated PML bodies are present in viable cells and are enriched in cells in the G(2)/M phase of the cell cycle. *J. Cell Sci*., **113 Pt 24**, 4577–4585.
58. Minocherhomji,S., Ying,S., Bjerregaard,V.A., Bursomanno,S., Aleliunaite,A., Wu,W., Mankouri,H.W., Shen,H., Liu,Y. and Hickson,I.D. (2015) Replication stress activates DNA repair synthesis in mitosis. *Nature*, **528**, 286–290.
59. Cho,N.W., Dilley,R.L., Lampson,M.A. and Greenberg,R.A. (2014) Interchromosomal homology searches drive directional ALT telomere movement and synapsis. *Cell*, **159**, 108–121.
60. Yang,Y., Jayaprakash,D., Hollingworth,R., Chen,S., Jablonski,A.E., Gao,Y., Anand,J.R., Mutter-Rottmayer,E., An,J., Cheng,X., *et al.* (2021) A degenerate PCNA-interacting peptide (DPIP) box targets RNF168 to replicating DNA to limit 53BP1 signaling. bioRxiv doi: https://doi.org/10.1101/2021.03.17.435897, 18 March 2021, preprint: not peer reviewed.
61. Sobinoff,A.P., Allen,J.A., Neumann,A.A., Yang,S.F., Walsh,M.E., Henson,J.D., Reddel,R.R. and Pickett,H.A. (2017) BLM and SLX4 play opposing roles in recombination-dependent replication at human telomeres. *EMBO J*., **36**, 2907–2919.
62. Cesare,A.J. and Griffith,J.D. (2004) Telomeric DNA in ALT cells is characterized by free telomeric circles and heterogeneous t-loops. *Mol. Cell. Biol*., **24**, 9948–9957.
63. Cesare,A.J., Kaul,Z., Cohen,S.B., Napier,C.E., Pickett,H.A., Neumann,A.A. and Reddel,R.R. (2009) Spontaneous occurrence of telomeric DNA damage response in the absence of chromosome fusions. *Nat. Struct. Mol. Biol*., **16**, 1244–1251.
64. Liang,Q., Dexheimer,T.S., Zhang,P., Rosenthal,A.S., Villamil,M.A., You,C., Zhang,Q., Chen,J., Ott,C.A., Sun,H., *et al.* (2014) A selective USP1-UAF1 inhibitor links deubiquitination to DNA damage responses. *Nat. Chem. Biol*., **10**, 298–304.
65. Takai,H., Smogorzewska,A. and de Lange,T. (2003) DNA damage foci at dysfunctional telomeres. *Curr. Biol*., **13**, 1549–1556.
66. Wojtaszek,J.L., Chatterjee,N., Najeeb,J., Ramos,A., Lee,M., Bian,K., Xue,J.Y., Fenton,B.A., Park,H., Li,D., *et al.* (2019) A small molecule targeting mutagenic translesion synthesis improves chemotherapy. *Cell*, **178**, 152–159.
67. Kim,Y., Lach,F.P., Desetty,R., Hanenberg,H., Auerbach,A.D. and Smogorzewska,A. (2011) Mutations of the SLX4 gene in Fanconi anemia. *Nat. Genet*., **43**, 142–146.
68. Lachaud,C., Castor,D., Hain,K., Munoz,I., Wilson,J., MacArtney,T.J., Schindler,D. and Rouse,J. (2014) Distinct functional roles for the two SLX4 ubiquitin-binding UBZ domains mutated in Fanconi anemia. *J. Cell Sci*., **127**, 2811–2817.
69. Wan,B., Yin,J., Horvath,K., Sarkar,J., Chen,Y., Wu,J., Wan,K., Lu,J., Gu,P., Yu,E.Y., *et al.* (2013) SLX4 assembles a telomere maintenance toolkit by bridging multiple endonucleases with telomeres. *Cell Rep*., **4**, 861–869.
70. Wilson,J.S., Tejera,A.M., Castor,D., Toth,R., Blasco,M.A. and Rouse,J. (2013) Localization-dependent and -independent roles of SLX4 in regulating telomeres. *Cell Rep*., **4**, 853–860.
71. Lee,K.Y. and Myung,K. (2008) PCNA modifications for regulation of post-replication repair pathways. *Mol. Cells*, **26**, 5–11.
72. Pulvino,M., Liang,Y., Oleksyn,D., DeRan,M., Van Pelt,E., Shapiro,J., Sanz,I., Chen,L. and Zhao,J. (2012) Inhibition of proliferation and survival of diffuse large B-cell lymphoma cells by a small-molecule inhibitor of the ubiquitin-conjugating enzyme Ubc13-Uev1A. *Blood*, **120**, 1668–1677.
73. Chan,K.L., Palmai-Pallag,T., Ying,S. and Hickson,I.D. (2009) Replication stress induces sister-chromatid bridging at fragile site loci in mitosis. *Nat. Cell Biol*., **11**, 753–760.
74. Munoz,I.M., Hain,K., Declais,A.C., Gardiner,M., Toh,G.W., Sanchez-Pulido,L., Heuckmann,J.M., Toth,R., Macartney,T., Eppink,B., *et al.* (2009) Coordination of structure-specific nucleases by human SLX4/BTBD12 is required for DNA repair. *Mol. Cell*, **35**, 116–127.
75. Zlatanou,A., Despras,E., Braz-Petta,T., Boubakour-Azzouz,I., Pouvelle,C., Stewart,G.S., Nakajima,S., Yasui,A., Ishchenko,A.A. and Kannouche,P.L. (2011) The hMsh2-hMsh6 complex acts in concert with monoubiquitinated PCNA and Pol eta in response to oxidative DNA damage in human cells. *Mol. Cell*, **43**, 649–662.

76. Helmrich,A., Ballarino,M. and Tora,L. (2011) Collisions between replication and transcription complexes cause common fragile site instability at the longest human genes. *Mol. Cell*, **44**, 966–977.
77. Macheret,M., Bhowmick,R., Sobkowiak,K., Padayachy,L., Mailler,J., Hickson,I.D. and Halazonetis,T.D. (2020) High-resolution mapping of mitotic DNA synthesis regions and common fragile sites in the human genome through direct sequencing. *Cell Res.*, **30**, 997–1008.
78. Lu,R. and Pickett,H.A. (2022) Telomeric replication stress: the beginning and the end for alternative lengthening of telomeres cancers. *Open Biol.*, **12**, 220011.
79. Wassing,I.E., Graham,E., Saayman,X., Rampazzo,L., Ralf,C., Bassett,A. and Esashi,F. (2021) The RAD51 recombinase protects mitotic chromatin in human cells. *Nat. Commun.*, **12**, 5380.
80. Deng,L., Wu,R.A., Sonneville,R., Kochenova,O.V., Labib,K., Pellman,D. and Walter,J.C. (2019) Mitotic CDK promotes replisome disassembly, fork breakage, and complex DNA rearrangements. *Mol. Cell*, **73**, 915–929.
81. Diamant,N., Hendel,A., Vered,I., Carell,T., Reissner,T., de Wind,N., Geacinov,N. and Livneh,Z. (2012) DNA damage bypass operates in the S and G2 phases of the cell cycle and exhibits differential mutagenicity. *Nucleic Acids Res.*, **40**, 170–180.
82. Wyatt,H.D., Laister,R.C., Martin,S.R., Arrowsmith,C.H. and West,S.C. (2017) The SMX DNA repair tri-nuclease. *Mol. Cell*, **65**, 848–860.
83. Gali,H., Juhasz,S., Morocz,M., Hajdu,I., Fatyol,K., Szukacsov,V., Burkovics,P. and Haracska,L. (2012) Role of SUMO modification of human PCNA at stalled replication fork. *Nucleic Acids Res.*, **40**, 6049–6059.
84. Hendriks,I.A., D'Souza,R.C., Yang,B., Vries,V.-d., M.,M. and Vertegaal,A.C. (2014) Uncovering global SUMOylation signaling networks in a site-specific manner. *Nat. Struct. Mol. Biol.*, **21**, 927–936.
85. Pfander,B., Moldovan,G.L., Sacher,M., Hoege,C. and Jentsch,S. (2005) SUMO-modified PCNA recruits Srs2 to prevent recombination during S phase. *Nature*, **436**, 428–433.
86. Singh,P., Gazy,I. and Kupiec,M. (2023) Control of telomere length in yeast by SUMOylated PCNA and the Elg1 PCNA unloader. *eLife*, **12**, RP86990.
87. Pennock,E., Buckley,K. and Lundblad,V. (2001) Cdc13 delivers separate complexes to the telomere for end protection and replication. *Cell*, **104**, 387–396.
88. Evans,S.K. and Lundblad,V. (1999) Est1 and Cdc13 as comediators of telomerase access. *Science*, **286**, 117–120.
89. Chandra,A., Hughes,T.R., Nugent,C.I. and Lundblad,V. (2001) Cdc13 both positively and negatively regulates telomere replication. *Genes Dev.*, **15**, 404–414.
90. Chen,L.Y., Redon,S. and Lingner,J. (2012) The human CST complex is a terminator of telomerase activity. *Nature*, **488**, 540–544.
91. Moldovan,G.L., Dejsuphong,D., Petalcorin,M.I., Hofmann,K., Takeda,S., Boulton,S.J. and D'Andrea,A.D. (2012) Inhibition of homologous recombination by the PCNA-interacting protein PARI. *Mol. Cell*, **45**, 75–86.

Received: September 4, 2023. **Revised:** August 23, 2024. **Editorial Decision:** August 25, 2024. **Accepted:** August 29, 2024